THE ASTROPHYSICAL JOURNAL, 302:138–162, 1986 March 1

WAVE PROPAGATION IN PULSAR MAGNETOSPHERES: REFRACTION OF RAYS IN THE OPEN FLUX ZONE

JOHN J. BARNARD[1]
Department of Astronomy, University of California at Berkeley, and Laboratory for High Energy Astrophysics, NASA-Goddard Space Flight Center

AND

JONATHAN ARONS
Department of Astronomy and Department of Physics, University of California at Berkeley, and Institute of Geophysics and Planetary Physics, University of California, Lawrence Livermore Laboratory
Received 1985 April 5; accepted 1985 July 18

ABSTRACT

We investigate the propagation of waves through a relativistically outflowing electron-positron plasma in a very strong dipolar magnetic field, conditions expected in pulsar magnetospheres. We derive Hamilton's equations for the propagation of rays through a plasma which is inhomogeneous in density, magnetic field direction, and Lorentz factor. We numerically and analytically solve these equations for rays propagating through the plasmas outflowing along the "open" dipolar field lines in which the density decreases inversely as the radius cubed and in the case where gradients transverse to the radial direction exist. In the radial case we determine the effects of refraction on pulse profiles, spectrum, and polarization, and indicate the effects of a transverse gradient. We examine models in which the observed broad bandwidth in the radio emission has its origin in a radius to frequency map. We also study models with broad-band emission at a single radius. We compare these to observations of pulse width and pulse component separation as a function of frequency. The origin of "orthogonal modes" is discussed.

Subject headings: hydromagnetics — polarization — pulsars — radiation mechanisms

I. INTRODUCTION

The development of models of pulsar magnetospheres containing dense, relativistic plasmas (Sturrock 1970, 1971; Ruderman and Sutherland 1975, hereafter RS; Cheng and Ruderman 1977, 1980; Arons and Scharlemann 1979, hereafter AS; Arons 1979, 1981, 1983*a*, *b*) has led a number of authors to consider the properties of wave propagation through such plasmas. For example, in a series of papers by Lerche and Lee (see, e.g., Lee and Lerche 1975, and references therein) ray paths and polarization characteristics were studied for a variety of geometries in which a large gradient in velocity was assumed. Although not directly related to polar cap models of pulsars, they pointed out the large effect that shearing relativistic plasmas can have on an incident radiation beam. Harding and Tademaru (1981, and references therein) investigated the effects of a shearing plasma on a pulse of radiation passing perpendicular to the direction of shear and found time-dependent modulation similar to observed microstructure (see, e.g., Cordes 1979).

The observation (see, e.g., Backer, Rankin, and Campbell 1976; Stinebring *et al.* 1984*a*, *b*, and references therein) that the polarization position angle at each pulse longitude is most likely to occur at two preferred values separated by $\sim 90°$ (so-called orthogonal modes) has also spurred investigation into propagation effects. Melrose and Stoneham (1977) and Melrose (1979) proposed that refraction can spatially separate beams with two different polarization states in the low-density limit and thus account for orthogonal modes. Blandford and Scharlemann (1976) invoke preferential Thomson scattering of one polarization state due to the anisotropic cross section in the intense magnetic field. Cheng and Ruderman (1979) propose two different emission mechanisms, "longitudinal emission" and curvature emission, together with the "combing" effect of the magnetic field ("adiabatic walking") to explain orthogonal modes.

In the accompanying paper (Arons and Barnard 1986, hereafter Paper I) we derived and evaluated in several regimes the dispersion relation for wave propagation in a relativistic plasma, in a superstrong magnetic field. In this paper we investigate the refraction of waves in these plasmas, using the results of Paper I, and generalize the work of Melrose and Stoneham (1977) into higher density regimes. We carry out detailed ray tracings through model pulsar magnetospheres, in order to make contact with observational data.

In § II we use the infinite magnetic field approximation of Paper I to find Hamilton's equations for wave trajectories. In § III we solve the ray equations for a number of simple but illustrative models of the density and momentum distribution of the outflowing plasma and some simple assumptions about the emission mechanism, calculating the consequences of these assumptions on pulse profiles and polarization. In § IV we discuss how some features of radio pulsar morphology may be related to refraction, and compare our simple hypotheses about the emission mechanism and plasma distribution with the observations. In § V we summarize these results and suggest some observational tests of our theory.

[1] Research Associate of the National Research Council.

II. HAMILTON'S EQUATIONS

In the pulsar models we are considering, the scale lengths in the radial direction are on the order of the radius of emission $\sim 10^8$ cm, and in the transverse direction, relevant length scales are the width of the open flux tube $\sim 10^7$ cm, the thickness of the "slot gap" is $\sim 10^6$ cm (as in Arons 1983*a*), and the width of the boundary layer between the slot gap and the pair plasma, $\sim 10^4$ cm, all scales which are much longer than the typical wavelength of the observed radio waves (~ 1–10^3 cm). Thus, in calculating the trajectories of wave packets the "slowly varying" or Eikonal approximation can be used (Weinberg 1962; Bekefi 1966) in which the wave properties are determined by the local plasma properties, but with the rate of change of the position, momentum, and frequency of the wave packet determined by the spatial, temporal, and wave vector gradients of the local dispersion relation. Thus if the dispersion relation is given by $D(\omega, k, x, t) = 0$, then the coordinates of a wave packet (in x, k, ω space) change in time according to

$$\frac{dx}{dt_r} = \frac{-\partial D/\partial k}{\partial D/\partial \omega}, \tag{1}$$

$$\frac{dk}{dt_r} = \frac{\partial D/\partial x}{\partial D/\partial \omega}, \tag{2}$$

$$\frac{d\omega}{dt_r} = \frac{-\partial D/\partial t}{\partial D/\partial \omega}. \tag{3}$$

Here t_r is the time elapsed since the creation of a wave packet measured in the laboratory frame. If the dispersion relation is independent of time, then the frequency is a constant, $0 = \omega - \omega(k, x) \equiv D$, so that

$$\frac{dx}{dt_r} = \frac{\partial \omega}{\partial k}(k, x), \tag{4}$$

$$\frac{dk}{dt_r} = \frac{-\partial \omega}{\partial x}(k, x). \tag{5}$$

In equations (4) and (5) $\omega(x, k)$ is given by the dispersion relation.

As discussed in Paper I, under the conditions of polar flow of pulsar emission zones, the radiation propagates in two independent normal modes. These are the ordinary, or O-mode, with linearly polarized electric field in the plane of k and B, and the extraordinary, or X-mode, with linearly polarized electric field perpendicular to the (k, B)-plane. In most regions of the polar flow, it is safe to assume the cyclotron frequencies vastly exceeds the Doppler-shifted frequencies of the waves. Then the refractive effects are adequately modeled by using dispersion relations derived as if the magnetic field were infinite. The X-mode propagates as if in a vacuum, with $\omega^2 = c^2k^2$. In the O polarization, ω and k are connected by the dispersion relation from Paper I:

$$D_0 = (\omega^2 - c^2k_\parallel^2)\left(1 - \sum_s \frac{\omega_s^2}{\omega^2} g_s\right) - c^2k_\perp^2 = 0, \tag{I.45}$$

with

$$g_s = P \int_{-\infty}^{\infty} \frac{du_\parallel f_s(u_\parallel)}{\gamma^3(1 - n_\parallel \beta_\parallel)^2}. \tag{I.46}$$

Here f_s is the distribution function of species s, $u_\parallel$ is the momentum of a particle moving along B as measured in units of $m_s c$, $n_\parallel = ck_\parallel/\omega$, $k_\parallel$ is the component of k along B, $\gamma = (1 + u_\parallel^2)^{1/2}$ and $\beta_\parallel = u_\parallel/\gamma$ is the speed along B. When the O-mode is subluminous ($n_\parallel > 1$), the integral in equation (I.46) is done in the principal value sense.

Differentiating with respect to x and k yields

$$\frac{1}{c}\frac{\partial \omega}{\partial k} = \left\{\left[(1 - n_\parallel^2)\sum_s \frac{\partial g_s}{\partial n_\parallel}\left(\frac{\omega_s}{\omega}\right)^2 - 2n_\parallel \sum_s g_s\left(\frac{\omega_s}{\omega}\right)^2\right]b + 2n\right\}$$
$$\div \left\{2\left[1 - \sum_s g_s\left(\frac{\omega_s}{\omega}\right)^2\right] + (1 - n_\parallel^2)\left[2\sum_s g_s\left(\frac{\omega_s}{\omega}\right)^2 + n_\parallel \sum_s \frac{\partial g_s}{\partial n_\parallel}\left(\frac{\omega_s}{\omega}\right)^2\right]\right\}, \tag{6}$$

$$\frac{1}{\omega}\frac{\partial \omega}{\partial x} = \left\{(1 - n_\parallel^2)\left[\sum_s \frac{\partial g_s}{\partial x}\bigg|_{n_\parallel}\left(\frac{\omega_s}{\omega}\right)^2 + \sum_s \frac{g_s}{\omega^2}\frac{\partial \omega_s^2}{\partial x}\right] + \left[\sum_s \left(\frac{\omega_s}{\omega}\right)^2 \frac{\partial g_s}{\partial n_\parallel}(1 - n_\parallel^2) - 2n_\parallel \sum_s \left(\frac{\omega_s}{\omega}\right)^2\right]\frac{\partial(n \cdot b)}{\partial x}\right\}$$
$$\div \left\{2\left[1 - \sum_s g_s\left(\frac{\omega_s}{\omega}\right)^2\right] + (1 - n_\parallel^2)\left[2\sum_s g_s\left(\frac{\omega_s}{\omega}\right)^2 + n_\parallel \sum_s \frac{\partial g_s}{\partial n_\parallel}\left(\frac{\omega_s}{\omega}\right)^2\right]\right\}. \tag{7}$$

We used the fact that

$$g_s = g_s[n_\parallel, f_s(x)],$$

and

$$n_{\parallel} = n_{\parallel}[x, k, \omega(x, k)] ,$$

so that

$$\left.\frac{\partial g_s}{\partial k}\right|_x = \left.\frac{\partial g_s}{\partial n_{\parallel}}\right|_{f_s} \left(\left.\frac{\partial n_{\parallel}}{\partial \omega}\right|_{k,x} \left.\frac{\partial \omega}{\partial k}\right|_x + \left.\frac{\partial n_{\parallel}}{\partial k}\right|_{\omega,x} \right) , \tag{8}$$

and

$$\left.\frac{\partial g_s}{\partial x}\right|_k = \left.\frac{\partial g_s}{\partial n_{\parallel}}\right|_{f_s} \left(\left.\frac{\partial n_{\parallel}}{\partial \omega}\right|_{k,x} \frac{\partial \omega}{\partial x} + \left.\frac{\partial n_{\parallel}}{\partial x}\right|_{k,\omega} \right) + \left.\frac{\partial g_s}{\partial x}\right|_{n_{\parallel}} . \tag{9}$$

Since $n_{\parallel} = c\boldsymbol{k} \cdot \boldsymbol{b}/\omega$, we have

$$\left.\frac{\partial n_{\parallel}}{\partial k}\right|_{\omega,x} = \frac{c\boldsymbol{b}}{\omega} ; \quad \left.\frac{\partial n_{\parallel}}{\partial \omega}\right|_{x,k} = \frac{-ck_{\parallel}}{\omega^2} , \quad \left.\frac{\partial n_{\parallel}}{\partial x}\right|_{k,\omega} = \frac{c}{\omega} \left.\frac{\partial(\boldsymbol{k} \cdot \boldsymbol{b})}{\partial x}\right|_k . \tag{10}$$

Equations (4) and (5) together with equations (6)–(10) are the first-order, nonlinear, coupled ordinary differential equations which describe the ray trajectories in a time-steady medium. The assumption of time independence of the plasma parameters (actually time independence in the corotating frame of the neutron star) is consistent with the time-steady models of pair formation (see, e.g., AS; Arons 1981, 1983*a*). This assumption is also consistent with "sparking" models (see, e.g., RS or Cheng and Ruderman 1980) when the fluctuations in density and other parameters due to the time-dependent behavior of the sparks is small. This can occur since many sparks will contribute to the density at any one place.

To evaluate equations (6) and (7) it is necessary to calculate $\sum_s \omega_s^2 \partial g_s/\partial n_{\parallel}$, $\sum_s g_s \delta\omega_s^2/\partial x$, and $\sum_s \omega_s^2 \partial g_s/\partial x$. We have done this for the cold plasma and hot waterbag distributions which we list in Appendix A.

Insertion of the top halves of equations (A1)–(A3) into equations (6) and (7) yields the ray equations for a cold plasma:

$$\frac{1}{c}\frac{dx}{dt_r} = p\boldsymbol{n} - q\boldsymbol{b} , \tag{11}$$

$$\frac{1}{\omega}\frac{dk}{dt_r} = q \left.\frac{\partial(\boldsymbol{b} \cdot \boldsymbol{n})}{\partial x}\right|_n - l\alpha \frac{\partial \ln N}{\partial x} + \alpha\left(3l - \frac{n_{\parallel}}{\beta_0 \gamma_0^2}\right) \frac{\partial \ln \gamma_0}{\partial x} . \tag{12}$$

Here $\alpha = \omega_p^2/(\gamma^3\omega^2)$, $p = (1 - n_{\parallel}\beta_0)^3/d$, $q = \alpha(n_{\parallel} - \beta_0)/d$, $l = (1 - n_{\parallel}^2)(1 - \beta_0 n_{\parallel})/(2d)$, and $d = (1 - n_{\parallel}\beta_0)^3 - \alpha n_{\parallel}(n_{\parallel} - \beta_0)$.

Since dx/dt is expressed in terms of the parallel component of $\boldsymbol{n}$, it is useful to write the time derivative of $\boldsymbol{k}$ (or $\boldsymbol{n}$) in terms of the components parallel and perpendicular to the magnetic field:

$$\frac{dn_{\parallel}}{dt_r} = \frac{d(\boldsymbol{n} \cdot \boldsymbol{b})}{dt_r} = \frac{d\boldsymbol{n}}{dt_r} \cdot \boldsymbol{b} + n \cdot \left(\frac{\partial \boldsymbol{b}}{\partial x} \cdot \frac{dx}{dt_r}\right) , \tag{13}$$

and

$$\frac{dn_{\perp}}{dt_r} = \frac{d}{dt_r}[(\boldsymbol{n} \times \boldsymbol{b}) \cdot \boldsymbol{e}_{\phi}] = \boldsymbol{e}_{\phi} \cdot \left[\frac{d\boldsymbol{n}}{dt_r} \times \boldsymbol{b} + \boldsymbol{n} \times \left(\frac{\partial \boldsymbol{b}}{\partial x} \cdot \frac{dx}{dt_r}\right)\right] . \tag{14}$$

Here $\boldsymbol{e}_{\phi}$ is the unit vector in the direction of the magnetic azimuth and $\partial \boldsymbol{b}/\partial x$ is the matrix in which the ijth component is $\partial b_i/\partial x_j$. Equation (14) applies only to rays which lie in a plane of constant azimuth.

In the limit $\omega \ll (1 + \beta_0)\gamma_0 \omega_p'$ (i.e., the slow branch of the O-mode or $\alpha \gg 1$) the dispersion relation reduces to

$$\omega = ck_{\parallel} , \tag{15}$$

and equation (11) becomes

$$\frac{1}{c}\frac{dx}{dt_r} = \boldsymbol{b} . \tag{16}$$

If the plasma is uniform in density and Lorentz factor γ_0, equation (12) becomes

$$\frac{1}{\omega}\frac{dk}{dt_r} = \frac{\partial(\boldsymbol{b} \cdot \boldsymbol{n})}{\partial x} . \tag{17}$$

If the magnetic field is circular with radius of curvature, ρ, then equations (13) and (14) become

$$\frac{dk_{\parallel}}{dt_r} = 0 , \quad \frac{dk_{\perp}}{dt_r} = \frac{ck_{\parallel}}{\rho} . \tag{18}$$

Thus equation (16) implies the group velocity vector is aligned with the magnetic field, and so the wave packet simply follows the field. This is a consequence of the plasma's ability to short out most of the electric field parallel to the magnetic field, so that

conservation of Poynting flux ensures that the light wave (propagating only through displacement current) propagates along the $\boldsymbol{B}$-field. In contrast, the $\boldsymbol{k}$ vector, for small path lengths, at least, remains fixed in space. That is, for a wave which is emitted along the field at time $t = 0$, at time t_0 it will have developed a perpendicular component $k_\perp = ck_{\|0}t_0/\rho$. The group velocity vector will have been deflected by an angle $\approx ct_0/\rho$. Thus, $\boldsymbol{k}$ remains fixed, approximately compensating for the changing direction of dx/dt. This is a consequence of the fact the field is curved and the phase velocity of the waves is essentially c. If the planes of constant phase are initially perpendicular to the field, the phase of the waves at larger distance from the center of curvature of the magnetic field will lag behind those that are close to the center of curvature. Consequently, the plane of constant phase gets more and more oblique to the field as the wave progresses, indicating a larger and larger value of $k_\perp$.

In the opposite limit, $\omega \gg (1 + \beta_0)\gamma_0\omega'_p$, $|\alpha(\beta_0 - n_\|)| \ll |(1 - \beta_0 n_\|)^3|$, and the group velocity vector can be approximately written

$$\frac{1}{c}\frac{dx}{dt_r} = \left[1 - \frac{\alpha n_\|(\beta_0 - n_\|)}{(1 - \beta_0 n_\|)^3}\right]\boldsymbol{n} + \frac{\alpha(\beta_0 - n_\|)}{(1 - \beta_0 n_\|)^3}\boldsymbol{b}\,. \tag{19}$$

The angle $\Delta\beta_g$ between the group velocity vectors of an X-mode and an O-mode wave with identical $\boldsymbol{k}$, (with the assumption that $n \approx 1$), is given by

$$\Delta\beta_g = \frac{\omega'^2_p}{\gamma_0^2\omega^2}\frac{\sin\theta_b(\beta_0 - \cos\theta_b)}{(1 - \beta_0\cos\theta_b)^3}\,. \tag{20}$$

Here θ_b is the angle between the magnetic field and $\boldsymbol{k}$. Equation (20) is identical to equations (25) and (20) in Melrose (1979). Evaluation of equation (20) at its maximum $\theta_b \approx 1/[2^{1/2}(1 + \beta_0)\gamma_0]$ yields a maximum $\Delta\beta_g \approx 0.9\gamma_0\omega'^2_p/\omega^2$. The physics of the separation of the O- and X-modes through the magnetosphere, however, depends on the gradients in the plasma parameters (i.e., $\boldsymbol{b}$, N, γ_0) which leads to angles quite different than are given above, particularly in the high-density regime.

III. APPLICATION TO IDEALIZED MAGNETOSPHERES

The final direction a wave packet takes as it leaves the magnetosphere is determined by the global distribution of the energy and density of the outflowing plasma and the direction and strength of the magnetic field. In addition, the stellar rotation introduces aberration and time delays, causing the angular separation of two different rays $\Delta\theta_R$ emitted at radial separation Δr of $\Delta\theta_R \approx \Delta r\Omega/c$ (Cordes 1978). We assume the neutron star is not rotating for the purposes of calculating the effects of refraction, which is appropriate if $\Delta\theta_R$ is much less than the angular change in ray direction due to refraction.

As a model of the outflowing plasma, we adopt "typical" electron zone pulsar parameters. A relativistic electron beam (density of $\sim[\Omega B/2\pi ce][R_*/r]^3 \approx 10^{11}[R_*/r]^3$ cm^{-3} and Lorentz factor $\gamma_0 \approx 10^6$) is accelerated from the stellar surface. The beam emits curvature radiation producing an electron-positron plasma, which is further enhanced in density by the conversion of the synchrotron radiation of the electron-positron plasma into more pairs, yielding a total density enhancement of 10^3–10^5 (RS; AS; Arons 1983*a*, *b*) over the original beam, and average Lorentz factor of $\sim$10–1000. Although the exact distribution along field lines is a function of the low-altitude ($r < 10R_*$) magnetic field geometry which may depart significantly from a purely dipole field (see, e.g., Barnard and Arons (1982), if the rotation frequency and field strength are significantly above pair creation threshold, the bulk of the plasma will have a density which is roughly independent of θ_*, the magnetic colatitude of the field lines at the stellar surface. However, as the outer boundary of the polar flux tube is approached, the potential in the corotating frame approaches the surface potential, greatly reducing the acceleration of the beam particles. The produces a "slot gap" (AS; Arons 1981, 1983*a*) on the boundary of the pair plasma. The gradients in plasma density and energy can be very large in this region where they are nearly transverse to the magnetic field, although extending over only a fraction of the width of the polar flux tube. In the radial direction, the plasma streams along the field lines. Conservation of particles and magnetic flux implies a number density proportional to magnetic field strength, which for a predominantly dipole field yields the r^{-3} dependence previously stated. We examine models with and without the transverse gradients in order to isolate the effect of the slot gap on final wave trajectories.

We also examine the assumption of broad-band emission at one altitude, emitted parallel to the magnetic field. This is in contrast to the radius-to-frequency mapping assumption which is commonly made (RS; Cordes 1978). Physically, if at a particular altitude, the emission occurs at $\omega' \approx \omega'_p$ in the rest frame, in the laboratory frame this emission is observed from $\omega \approx \omega'_p/\gamma_0$ to $\omega \approx 2\gamma_0\omega'_p$ on the superluminous branch of the O-mode. Further, if the radio emission results from the plasma instability associated with shear in the narrow transition region between the slot gap and the bulk of the pair plasma (see Arons 1983*a*), in which a range of plasma energy, density, and plasma frequency is present, the unstable plasma modes will be effectively broad band as they propagate into the column of the pair plasma.

a) Radial Density Gradient

i) Ray Trajectories

We consider a magnetic dipole aligned along the z-axis. In the (y-z)-plane, the y- and z-components of the field are given by

$$B_y = \frac{3}{2}B_d\left(\frac{R}{r}\right)^3\frac{zy}{r^2} \quad \text{and} \quad B_z = B_d\left(\frac{R}{r}\right)^3\left[1 - \frac{3y^2}{2r^2}\right]. \tag{21}$$

In general, the density is a function of field line and magnetic field strength:

$$N_p = N_{p0}(\theta_*)(B/B_*) \approx N_{p0}(\theta_*)(R_*/r)^3\ ; \tag{22}$$

$f_s(p_\parallel)$ is not a function of position for the present calculations. As indicated by the solution to equation (18), the field line curvature can increase $n_\perp$ from initially close to zero to of order θ. Since θ will be less than the pulse width of pulsars ($\sim 15°$), $n_\perp$ and θ can be treated as small parameters. Evaluating equations (11)–(14) and retaining terms linear in $n_\perp$ and θ yields

$$\frac{1}{c}\frac{dn_\perp}{dt_r} = -\left(\frac{3n_\perp}{2r} - \frac{3\theta n_\parallel}{4r}\right)(pn_\parallel - q) - \frac{l\alpha 3\theta}{2r}, \tag{23}$$

$$\frac{1}{c}\frac{dn_\parallel}{dt_r} = \frac{3l\alpha}{r}, \tag{24}$$

$$\frac{1}{c}\frac{dr}{dt_r} = pn_\parallel - q, \tag{25}$$

$$\frac{r}{c}\frac{d\theta}{dt_r} = \frac{\theta}{2}(pn_\parallel - q) - pn_\perp. \tag{26}$$

Here we have included a radial density gradient only (N_{p0} = constant). These equations can be further simplified by eliminating the time dependence, i.e. by dividing equations (23) and (26) by equation (25) and using the dispersion relation (46) of Paper I rather than equation (24) for $n_\parallel$:

$$r\frac{dn_\perp}{dr} = \frac{3\theta n_\parallel}{4} - \frac{3n_\perp}{2} - \frac{3\theta l\alpha}{2(pn_\parallel - q)}, \tag{27}$$

$$r\frac{d\theta}{dr} = \frac{\theta}{2} - \frac{n_\perp}{n_\parallel - q/p}. \tag{28}$$

Equations (27) and (28) may be solved analytically in three regimes: (1) the Alfvén mode (≡subluminous O-mode) at high density ($4\gamma_i^4\alpha \gg 1$); (2) the fast mode, at high density and small $n_\perp$ ($\alpha^{1/2} \gg n_\perp^2/2$); and (3) the fast mode (≡superluminous O-mode), at low density or large $n_\perp$ ($\alpha^{1/2} \ll n_\perp^2/2$). Table 1 lists the approximate expressions for p, q, and l which are correct through first order in $n_\perp$ and θ, in the three regimes. Insertion of these expressions into equations (27) and (28) yields (through first order in $n_\perp$ and θ):

$$r\frac{dn_\perp}{dr} = \frac{3\theta}{4} - \frac{3n_\perp}{2}, \tag{29}$$

$$r\frac{d\theta}{dr} = \frac{\theta}{2} - \sigma n_\perp. \tag{30}$$

Here $\sigma = 0, \frac{1}{2}, 1$ for the slow, high-density fast, and low-density fast modes, respectively. For simplicity we are considering rays confined to one magnetic azimuth. The full three-dimensional problem is found in Appendix B.

Equations (29) and (30) have parametric solution:

$$\frac{r}{r_0} = \left(\frac{u_0 - u_+}{u - u_+}\right)^{-a}\left(\frac{u_0 - u_-}{u - u_-}\right)^{a}, \tag{31}$$

$$\frac{\theta}{\theta_0} = \left(\frac{u_0 - u_+}{u - u_+}\right)^{(1+a)/2}\left(\frac{u_0 - u_-}{u - u_-}\right)^{(1-a)/2}, \tag{32}$$

$$n_\perp = u\theta. \tag{33}$$

Here the parameter u varies from u_0 to u_-, and the constants are $u_0 = n_{\perp 0}/\theta_0$; $u_\pm = \{1 \pm [1 - (3\sigma/4)]^{1/2}\}/\sigma$; and $a = 1/(4 - 3\sigma)^{1/2}$.

For the cases $\sigma = 0$ and 1, θ and $n_\perp$ can be expressed explicitly as functions of r. Note that positive $n_\perp$ is taken to be in the direction toward the magnetic axis.

TABLE 1

APPROXIMATE VALUES OF PARAMETERS IN EQUATIONS (27) AND (28)

Definition of Regime	Slow Mode at High Density $4\gamma_i^4\alpha \gg 1$ $n_\parallel \geq 1$	Fast Mode at High Density $1 > \alpha^{1/2} \gg n_\perp^2/2$ $n_\parallel \leq 1$	Fast Mode at Low Density $\alpha^{1/2} \ll n_\perp^2/2 \leq 1$ $n_\parallel \leq 1$
$n_\parallel$	1	$1 - \alpha^{1/2}$	1
σ	0	$\frac{1}{2}$	1
p	0	$\frac{1}{2}$	1
q	-1	$-\frac{1}{2}$	0
$l\alpha$	0	$\alpha^{1/2}/2$	0

$a =$ $\frac{1}{(4-3\sigma)^{1/2}}$ $\frac{1}{2}$ .63 1

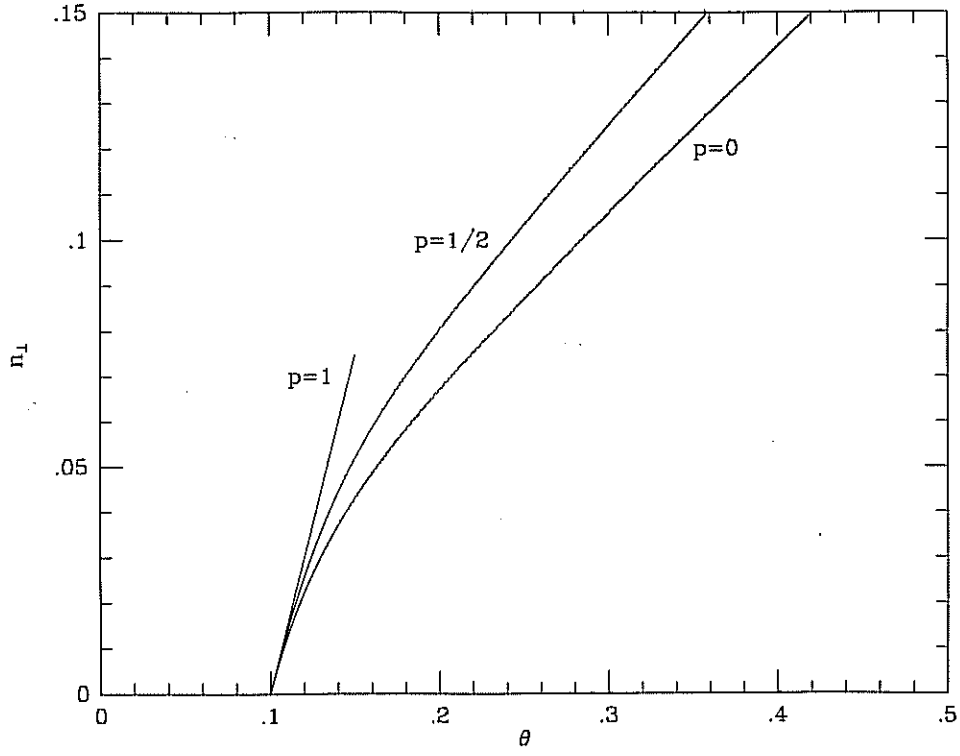

FIG. 1.—$n_\perp$ vs. θ for the solution to the linearized (in $n_\perp$, θ, and $1 - n_\parallel$) Hamiltons equations (eqs. [32] and [33]). For $p = 1$, $n_\perp$ reaches a maximum value since θ reaches a maximum (see eq. [64]).

$\sigma = 0$ (Alfvén mode):

$$\frac{\theta}{\theta_0} = \left(\frac{r}{r_0}\right)^{1/2}, \qquad n_\perp = \frac{3\theta_0}{8}\left(\frac{r}{r_0}\right)^{1/2} - \left(\frac{3\theta_0}{8} - n_{\perp 0}\right)\left(\frac{r}{r_0}\right)^{-3/2}. \tag{34}$$

$\sigma = 1$ (fast mode, low-density limit):

$$\frac{\theta}{\theta_0} = \frac{3}{2} - \frac{n_{\perp 0}}{\theta_0} + \frac{r_0}{r}\left(\frac{n_{\perp 0}}{\theta_0} - \frac{1}{2}\right), \qquad n_\perp = \frac{3\theta_0}{4} - \frac{n_{\perp 0}}{2} - \frac{3}{2}\left(\frac{r_0}{r}\right)\left(\frac{\theta_0}{2} - n_{\perp 0}\right). \tag{35}$$

Note that in equation (34) the wave trajectory is along a magnetic field line, while in equation (35) the wave simply follows straight unrefracted trajectories with fixed k vectors. For $\sigma = \frac{1}{2}$ (fast mode, high density) there is an intermediate trajectory. Noting that the first term in parentheses in equations (31) and (32) varies from 1 to 1.13 (for $\sigma = \frac{1}{2}$) as u varies from u_0 to u_-, whereas the second term varies from 1 to ∞ over the same range, the first term may be regarded as constant ≈ 1. Then the explicit solution is

$$\frac{\theta}{\theta_0} = v_1\left(\frac{r}{r_0}\right)^{(1-a)/2a},$$

$$n_\perp = u_- v_1\theta_0\left(\frac{r}{r_0}\right)^{(1-a)/2a} - \theta_0(u_- - u_0)\left(\frac{r}{r_0}\right)^{-(a+1)/2a}. \tag{36}$$

Here $v_1 \equiv (u_0 - u_+)/(u - u_+) \approx 1$, and, for $\sigma = \frac{1}{2}$, $a \approx 0.63$ and $u_- \approx 0.42$. Equation (36) approaches the exact solution as $\sigma \to 0$ and is still quite accurate for $\sigma = \frac{1}{2}$.

We have plotted $n_\perp$ versus θ and r versus $r\theta$ for the three cases in Figures 1 and 2.

As indicated by equation (34), wave packets on the slow branch at high density tend to follow the field lines, i.e. be "ducted" along the field. This tends to separate O-mode from X-mode spatially since the X-mode propagates as if unaffected by the field or the plasma, with straight ray paths identical to the fast low-density O-mode as in equation (22). However, as the Alfvén O-mode waves propagate outward, in the plasma of decreasing density, the wave frequency in the comoving frame approaches the comoving plasma frequency. As this occurs, the phase velocity of the wave parallel to the magnetic field decreases until it is equal to the velocity of electrons and positrons in the main body of the distribution function, causing the wave to be severely Landau damped before it can propagate to infinity (Paper I). Unless there is energy transfer from the slow mode to the fast mode, energy in this wave mode will not be observed. However, *if* energy transfer occurs at a frequency of the order of the comoving plasma frequency and it occurs in a region small compared to the scale over which the comoving plasma frequency varies, then there will be a radius $r_{\rm trans}$ below which waves will travel primarily along field lines and above which waves will travel essentially in straight lines in the direction of the constant k vector. Physical processes, such as wave-wave coupling and linear-gradient coupling which transfer

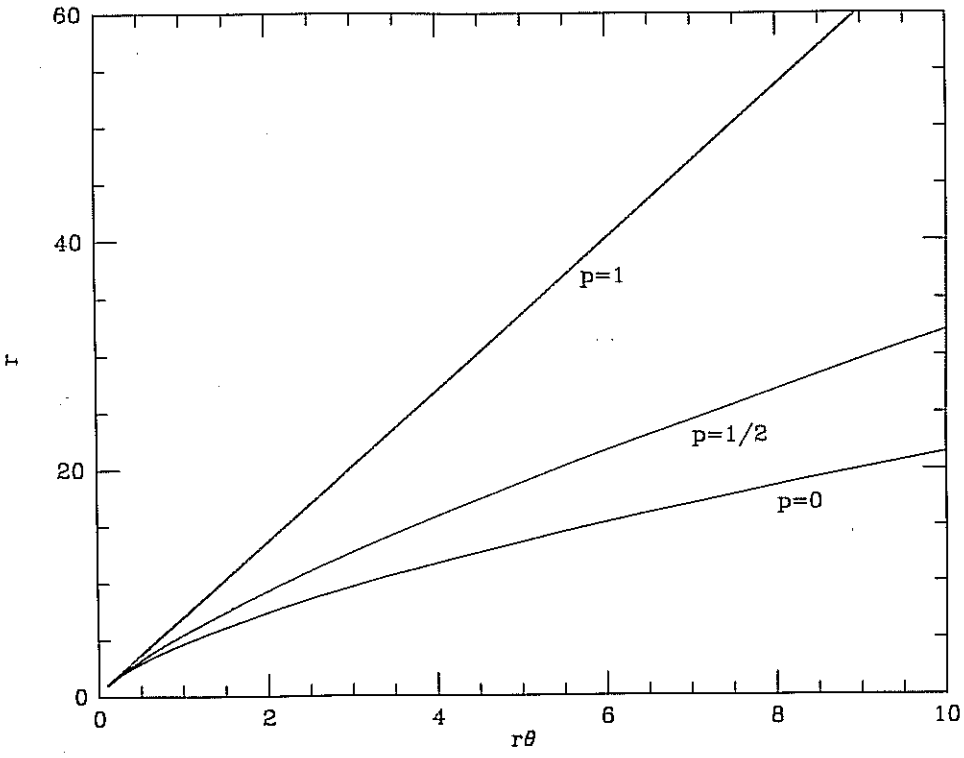

FIG. 2.—r vs. $r\theta$ from eqs. (31) and (32). (Through first order in θ this is identical to y vs. x.)

energy from one mode to another are currently under investigation by the authors. The angle between the dipole axis and the final ray direction ξ_f will have frequency dependence proportional to $\omega^{-1/3}$ (since $\omega_p' \approx N_p^{1/2} \approx [r/r_0]^{-3/2} \approx [\theta/\theta_0]^{-3}$). This exactly mimicks the radius to frequency mapping (see, e.g., RS) since an "emission" radius is simply replaced by a "transition" radius.

If wave energy originates on the fast branch, then the phase velocity is always greater than the particle velocities so that Landau damping does not occur. Emission directly onto this branch requires an intrinsically nonlinear process. At high densities and small values of $n_\perp$ the waves are Langmuir-like with superluminous phase velocities. As in the case of the slow mode, planes of constant phase lie close to planes of constant r since the phase velocity (see eq. [I.70]) depends primarily on r (through $\alpha^{1/2}$) and only in second order depends on θ (through $n_\perp^2$). Thus a component of k perpendicular to the magnetic field of order $k\theta$ is generated upon change of magnetic field direction of order θ. But as $k_\perp$ is increased, the wave becomes more and more electromagnetic, and the wave decouples from the plasma, subsequently following a straight wave trajectory. Prior to this decoupling the Langmuir disturbances to a large extent are convected with the plasma, since their group velocities in the comoving frame are much less than the plasma fluid velocity. Since the plasma is constrained to follow the field, to a large extent these waves do also.

We may estimate the final angle ξ_f with respect to the magnetic dipole $\boldsymbol{\mu}$ that a wave packet takes as it leaves the magnetosphere. From equation (36), $(\theta/\theta_0) \approx (r/r_0)^{0.29}$, indicating a ray trajectory which curves somewhat more slowly than a magnetic field line. To understand the evolution of the $\boldsymbol{k}$ vector in a heuristic way it is convenient to consider a plane of constant phase. Assume that $\boldsymbol{k}$ is initially parallel to $\boldsymbol{b}$. Then we may construct a plane of constant wave phase which lies perpendicular to the magnetic field and passes through r_0, θ_0. Since the phase velocity, through first order in θ, does not depend on the magnetic field direction, lines of constant phase will propagate in approximately straight lines. But since the magnetic field curves, $n_\perp$ will be of the same order as the change in angle of the magnetic field as is reflected in equation (36). As $n_\perp$ grows and as $\alpha^{1/2}$ decreases, the wave becomes less and less Langmuir-like and more and more like a light wave. The transition radius occurs when $n_\perp^2 \approx 2\alpha^{1/2}$ above which the wave disturbance travels (through first order) in a straight line.

Thus at this refraction-limiting radius (RLR) (indicated by subscript f):

$$\frac{\xi_f}{\theta_0} = \frac{3\theta_f}{2\theta_0} - \frac{n_{\perp f}}{\theta_0}, \tag{37}$$

where θ_f and $n_{\perp f}$ satisfy

$$0 = 1.41\alpha_0^{1/4}\left(\frac{\theta_f}{\theta_0}\right)^{-2.58} v_1^{2.58} - 0.42\theta_f - 0.42\theta_0\left(\frac{\theta_f}{\theta_0}\right)^{-4.44} v_1^{4.44}. \tag{38}$$

At large densities, $\theta_f/\theta_0 \gg 1$, so that $n_{\perp f} \approx 0.42\theta_f$, yielding

$$\frac{\xi_f}{\theta_0} \approx 1.66\theta_0^{-0.279}\alpha_0^{0.070}. \tag{39}$$

This power law in frequency occurs until $(\xi_f/\theta_0) \approx 3/2$ which from equation (39) yields a break frequency $\omega_{\rm br}$ of

$$\frac{\omega_{\rm br}}{\omega_{p0}} = 2.1\theta_0^{-2}\langle\gamma^{-3}\rangle^{1/2} = 4.7\xi_f^{-2}\langle\gamma^{-3}\rangle^{1/2} . \quad (40)$$

At frequencies above $\omega_{\rm br}$, the waves are unaffected by the plasma, so that ξ_f is essentially along the direction of the original k-vector, which is at an angle of $3/2\theta_0$ from the magnetic axis.

In Figures 3 and 4 we plot log ξ_f versus log ω/ω_{p0}, for the solution of equation (37) and (38), which has asymptotic behavior as in equations (39) and (40). In addition, we have numerically solved the nonlinear Hamilton's equations (eqs. [6] and [7] for the hot water bag (Fig. 4) and equations (11) and (12) for the cold plasma (Fig. 3).

Figure 3 shows that the linear solution agrees well with the numerical solution for large values of γ_0. As γ_0 decreases, however, $1 - n_\parallel$ becomes comparable to $1/\gamma_0^2$. From Paper I, equation (68), we noted that if $n_\perp < 1/\gamma_t$ and $\omega^2/\omega_p^2 > 4\langle\gamma\rangle$, then equation 67a of Paper I is the appropriate dispersion relation, and equation (70) of Paper I gives the corresponding phase velocity. Since the phase velocity increases with $n_\perp$, phase fronts far from the magnetic axis overtake those close to the axis causing the k vectors to be bent toward the magnetic axis. Only when γ_0 is relatively small so that $n_\perp$ can be relatively large and still be in the regime where refraction toward the axis takes place, can this occur. For larger γ, by the time α falls to below $\frac{1}{4}\gamma_t^4$, $n_\perp$ is greater than $1/\gamma_t$, so that a wave never enters this regime. The linear solution assumed that $1 - n_\parallel \approx \alpha^{1/2} \gg \frac{1}{2}\gamma^2$, and so does not agree well with the exact numerical solution for small γ_0. In Figure 4, again, for large upper cutoff the linear and numerical solutions agree, but since the lower cutoff ($\gamma_{\rm min} = 10$) increases the magnitude of the above effect, the linear solution slightly overestimates the refracted angle and again becomes inaccurate when $\gamma_{\rm max} \lesssim 10$.

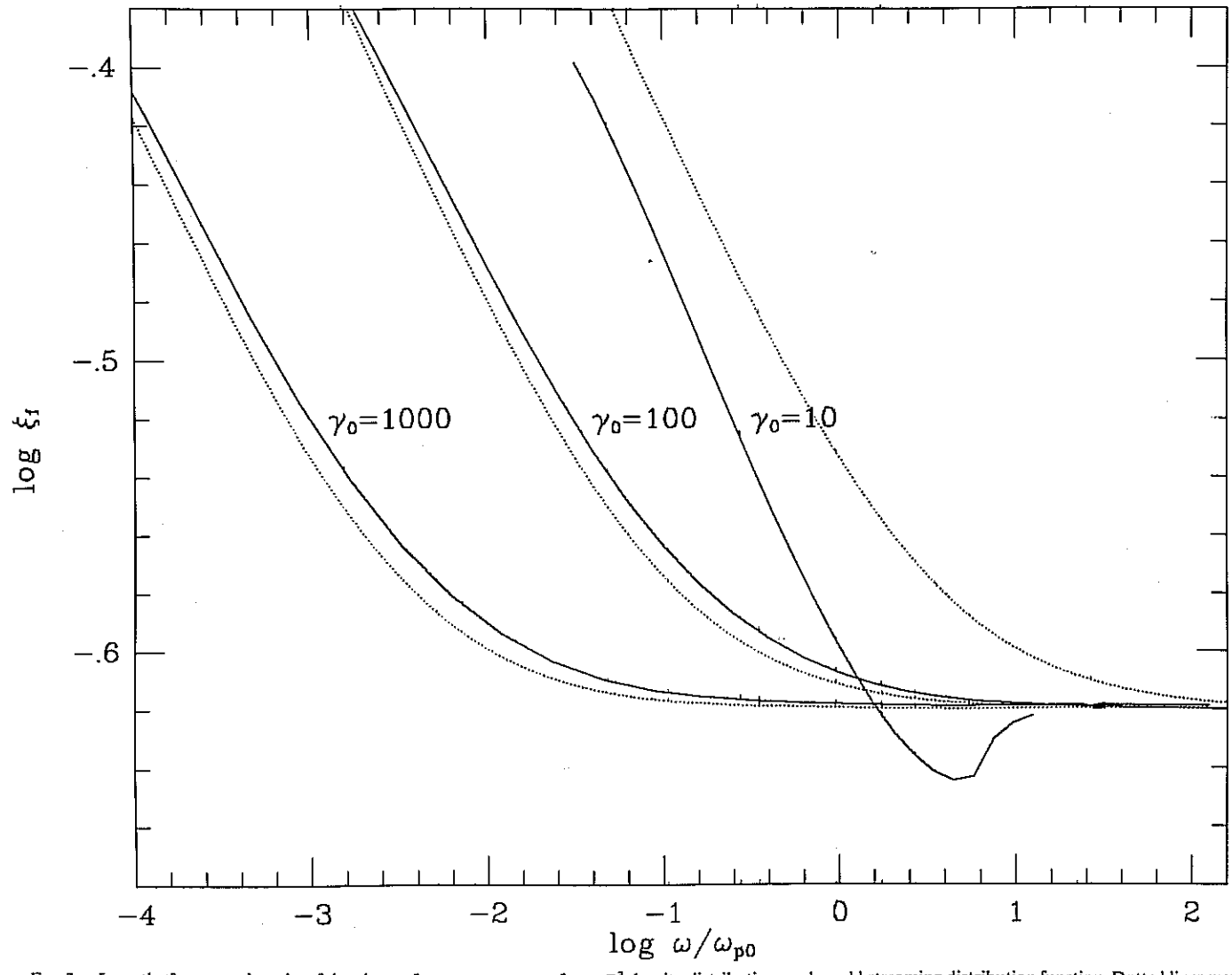

FIG. 3.—ξ_f vs. the frequency in units of the plasma frequency at $r = r_0$ for a r^{-3} density distribution, and a cold streaming distribution function. Dotted lines were found analytically from eq. (38), while the solid lines represent the numerical integration of the exact nonlinear Hamilton equations.

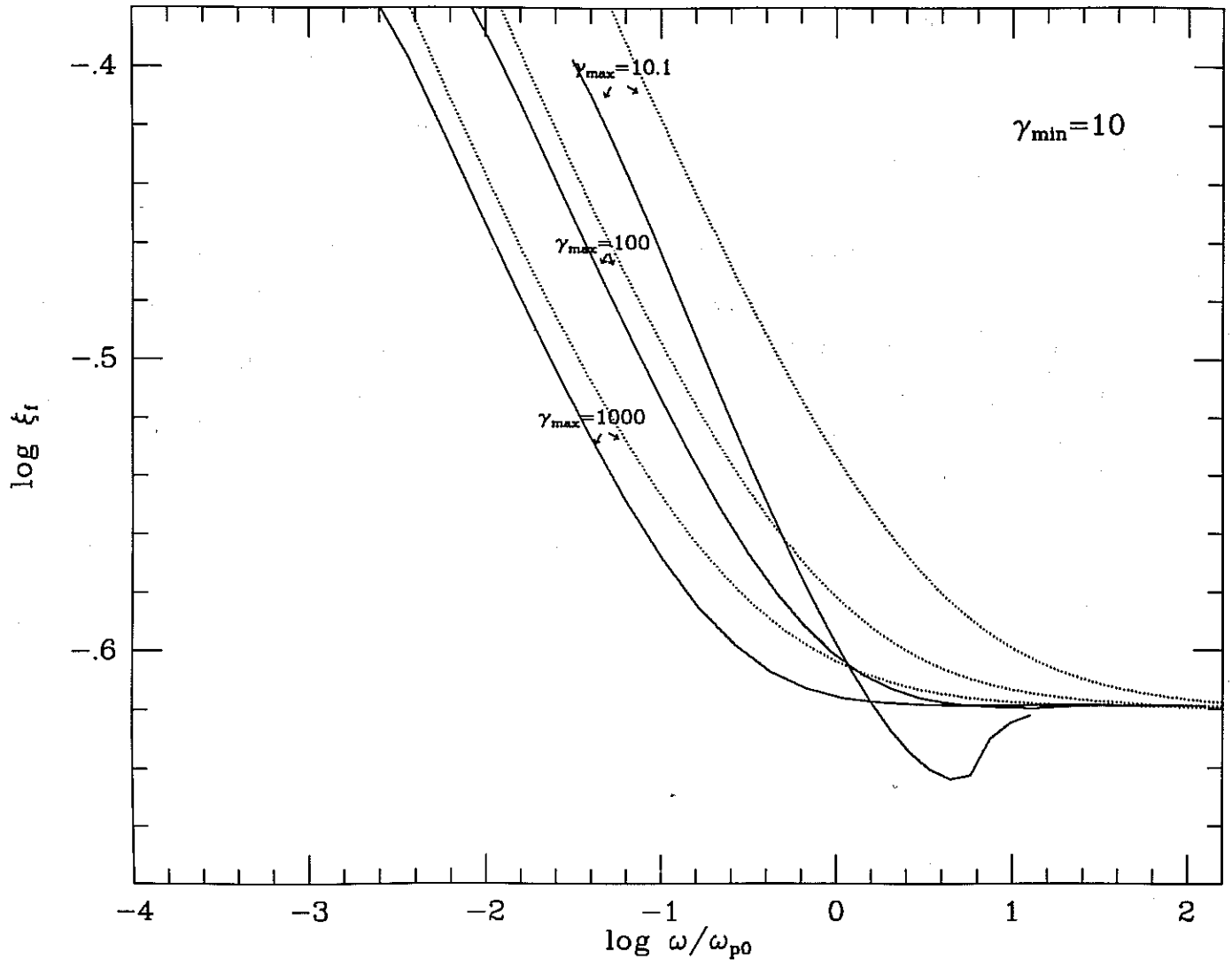

FIG. 4.—Same as in Fig. 3, except that a waterbag distribution function was used, with a minimum cutoff of $\gamma_{min} = 10$ and maximum cutoffs as indicated

ii) *Pulse Profiles*

Although the final ray directions give an indication of the broadening of pulse profiles due to refraction, more direct comparison with radio data requires integration of the emissivity over the entire open flux zone. The equation of radiative transfer in an anisotropic plasma is given by Bekefi (1966):

$$\frac{d}{dl}\left(\frac{I_\omega}{n_r^2}\right) = \frac{j_\omega}{n_r^2} - \frac{\kappa_\omega I_\omega}{n_r^2} . \tag{41}$$

Here I_ω is the energy passing unit area in unit time and in unit frequency bandwidth per unit solid angle in the direction of the group velocity vector, β_g, κ_ω is the opacity, and dl is a line element along a ray. The quantity n_r is the ray refractive index, which from Bekefi (1966) is

$$n_r^2 = \left| n^2 \sin\theta_b \left[1 + \left(\frac{1}{n}\frac{\partial n}{\partial \theta_b} \right)^2 \Big|_\omega \right]^{1/2} \left\{ \frac{\partial}{\partial \theta_b} \left[\frac{\cos\theta_b (n^{-1}\partial n/\partial\theta_b)|_\omega \sin\theta_b}{[1 + (n^{-1}\partial n/\partial\theta_b)^2|_\omega]^{1/2}} \right] \right\} \right| . \tag{42}$$

Far from the pulsar (when $n_r = 1$), the intensity is

$$I_\omega = \int \frac{j_\omega(l) dl}{n_r^2} , \tag{43}$$

where the integration is along a ray. We consider slowly rotating pulsars in the sense that angular aberration and time retardation effects are small compared to subpulse angles and time scales (as in Cordes 1978). Thus it is sufficient to calculate the intensity as a function of direction, n_f, with respect to the magnetic axis, and then to consider the rotation of this pattern of intensity in order to calculate the flux at a fixed point in space.

As a function of direction, $\boldsymbol{n}_f$, the flux is

$$F_\omega(\boldsymbol{n}_f, d) = \int I_\omega(\boldsymbol{n}_f, d)d\Omega = d^{-2} \int I_\omega(n_f, d)dA \ . \tag{44}$$

Here dA is an element of area perpendicular to $\boldsymbol{n}_f$ near the pulsar, and d is the distance to the observer. Using $dz = \boldsymbol{\beta}_{\rm gi} \cdot \boldsymbol{\beta}_{\rm gf}\, dl$, where dz is a displacement in the direction $\boldsymbol{n}_f$ and $\boldsymbol{\beta}_{\rm gi}$ is the initial direction of a ray which has final direction $\boldsymbol{\beta}_{\rm gf}$ ($\equiv \boldsymbol{n}_f$), the flux can be written:

$$F_\omega(\boldsymbol{n}_f, d) = \frac{1}{d^2} \int \frac{j_\omega[r, \beta_{\rm gi}(\boldsymbol{n}_f)]dV}{n_r^2 \boldsymbol{n}_f \cdot \boldsymbol{\beta}_{\rm gi}(\boldsymbol{n}_f)} \ , \tag{45}$$

where dV is an element of volume.

It is beyond the purpose of this paper to calculate the emissivity either as a function of position or direction for any hypothetical emission mechanism. Yet to maintain as general a discussion as possible we allow a power-law distribution of emissivity in r, θ_*, and ω/ω_p with upper and lower limits (denoted by subscripts "max" and "min," respectively) for each variable. In addition, we assume that the emissivity is highly beamed along the magnetic field, so that

$$j_\omega(r, \eta_i, \xi_i) = \begin{cases} j_0\, \delta(\Phi) \dfrac{\delta(\Theta)}{\sin \xi_i} \left(\dfrac{\omega}{\omega_p}\right)^{\alpha_\omega} \left(\dfrac{r}{r_0}\right)^{\alpha_r} \left(\dfrac{\theta_*}{\theta_{*\max}}\right)^{\alpha_\theta} & r_{\min} < r < r_{\max} \\ & \text{if} \quad \theta_{*\min} < \theta_* < \theta_{*\max} \\ & \left(\dfrac{\omega}{\omega_p}\right)_{\min} < \left(\dfrac{\omega}{\omega_p}\right) < \left(\dfrac{\omega}{\omega_p}\right)_{\max} \\ 0 & \text{otherwise} \end{cases} \tag{46}$$

Here (ξ_i, η_i) are the polar angles of the initial unit wave vector $\boldsymbol{n}_i$ at the initial position r_0 having spherical coordinates (r_0, θ_0, ϕ_0) (see Fig. 5). Also, $\Phi \equiv \eta_i - \phi_0$, and $\Theta \equiv \xi_i - 3\theta_0/2$.

Making use of the dipolar geometry and equation (22), the upper expression in equation (46) becomes

$$j_\omega = j_0\, \delta(\Phi) \frac{\delta(\Theta)}{\sin \xi_i} \left(\frac{\omega}{\omega_0}\right)^{\alpha_\omega} \left(\frac{\theta_0}{\theta_{*\max}}\right)^{\alpha_\theta} \left(\frac{r}{r_0}\right)^{(\alpha_r - \alpha_\theta)/(2 + 3\alpha_\omega/2)} \ . \tag{47}$$

Here ω_0 is the plasma frequency at radius r_0.

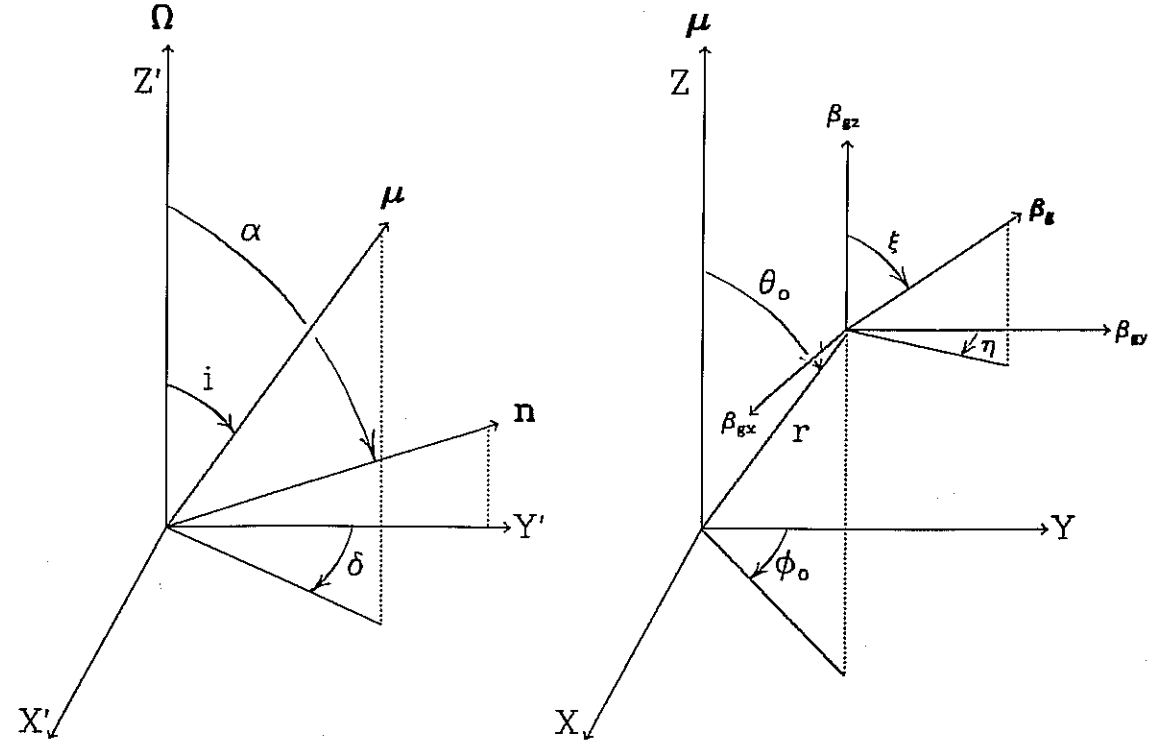

FIG. 5.—Orientation of various angles and axes. *Left*: dipole moment $\boldsymbol{\mu}$ is inclined by the angle i from the rotation axis $\boldsymbol{\Omega}$, while the line of sight is in the direction $\boldsymbol{n}$ and is inclined by the angle α from $\boldsymbol{\Omega}$. As the pulsar rotates, the rotational phase angle δ continually grows. *Right*: At the position r with spherical coordinates (r, θ_0, ϕ_0) the group velocity vector $\boldsymbol{\beta}_g$ is designated by the spherical angles (ξ, η) in the rotating frame of the pulsar. At the RLR $\boldsymbol{\beta}_{gf}$ must be parallel to $\boldsymbol{n}$ in order to reach the observer.

As indicated in equation (45), the initial direction of the ray is considered a function of the final direction as well as the coordinates. Thus $\xi_i = \xi_i(\xi_f, \eta_f, \theta_0, \phi_0)$ and $\eta_i = \eta_i(\xi_f, \eta_f, \theta_0, \phi_0)$. For the case of a radial density gradient, and for a ray which is emitted along the field ($\Phi = \Theta = 0$) equation (39) is sufficiently accurate in the high-density limit, and $\xi_i = \xi_f = 3\theta_0/2$ in the low-density limit. Thus including the radial dependence of the density explicitly we have (for $n_\perp = 0$):

$$\xi_i = \begin{cases} \frac{3}{2}\xi_f^{1/m} a^{-1/m} (r/r_0)^{-n/m} & \text{for } r < r_{\omega t} \\ \xi_f & \text{for } r > r_{\omega t} \end{cases} . \tag{48}$$

Here $m = 0.721$, $n = -0.210$, $a = 1.66\alpha_0^{0.07}$, and $r_{\omega t} = [(3/2)^m(\xi_f^{1-m})/a]^{1/n} r_0$. The volume element dV in equation (45) in polar coordinates is $r^2 \sin\theta_0\, d\theta_0\, d\phi_0\, dr$. Integration of equation (45), with equation (46) used for the emissivity, over θ_0 and ϕ_0 yields the radial integral:

$$F_\omega(n_f, d) = \frac{2}{3} j_0 \left(\frac{r_0}{d}\right)^2 \left(\frac{\omega}{\omega_0}\right)^{\alpha_\omega} \int dr \left[\frac{2\xi_i(\xi_f, r)}{3\theta_{*\max}}\right]^{\alpha_\theta} \left(\frac{r}{r_0}\right)^{\alpha_{r_1}} \left[n_r^2 \cos(\xi_i - \xi_f) \left|\frac{\partial\Theta}{\partial\theta_0}\frac{\partial\Phi}{\partial\phi_0} - \frac{\partial\Theta}{\partial\phi_0}\frac{\partial\Phi}{\partial\theta_0}\right|\right]^{-1} , \tag{49}$$

where the integration limits are chosen such that the constraints on equation (46) are met. Here $\alpha_{r_1} = \alpha_r - \alpha_\theta/2 + 3\alpha_\omega/2 + 2$. The Jacobian in the absolute value sign is evaluated at $\Theta = \Phi = 0$, and with ξ_f and η_f held constant. In order to evaluate this Jacobian, we need to have ray trajectories, which are not emitted parallel to the field nor even constrained to lie in an azimuthal plane. These solutions are obtained in Appendix B. Since the solution gives the final values of the coordinates and the ray directions as functions of the initial values, whereas the derivatives in equation (49) are of the initial values of the direction with respect to the initial values of the coordinates, keeping the final values of the direction constant, some algebraic manipulation is required and is outlined in Appendix C. The result in the high- and low-density limits is

$$\left|\frac{\partial\Theta}{\partial\theta_0}\frac{\partial\Phi}{\partial\phi_0}\frac{\partial\Theta}{\partial\phi_0}\frac{\partial\Phi}{\partial\theta_0}\right|^{-1} = \begin{cases} 2u_-/u_+ & \text{for } r < r_{\omega t} \\ \frac{2}{3} & \text{for } r > r_{\omega t} \end{cases} . \tag{50}$$

Since the emissivity is nonzero only along the field direction, $n_r^2 = n_\parallel^2 \approx 1$. Because ξ_i and ξ_f are both small, $\cos(\xi_i - \xi_f) \approx 1$. Evaluation of the radial integral in equation (45) is straightforward in the two limits in equations (48) and (49) as long as careful consideration is paid to the integration limits. The result of the radial integration is

$$F_\omega(\xi_f, \eta_f, d) = \frac{2}{3}\left(\frac{\omega}{\omega_0}\right)^{\alpha_\omega} \frac{j_0 r_0^3}{d^2 \theta_{*\max}^{\alpha_\theta}} \begin{cases} 0 & r_{\text{up }1} < r_{\text{low }1} \text{ and } r_{\text{up }2} < r_{\text{low }2} \\ I_1 & r_{\text{up }1} > r_{\text{low }1} \text{ and } r_{\text{up }2} < r_{\text{low }2} \\ I_2 & r_{\text{up }1} < r_{\text{low }1} \text{ and } r_{\text{up }2} > r_{\text{low }2} \\ I_1 + I_2 & r_{\text{up }1} > r_{\text{low }1} \text{ and } r_{\text{up }2} > r_{\text{low }2} \end{cases} . \tag{51}$$

Here

$$I_1 \equiv \frac{2u_-}{\alpha_1 u_+}\left(\frac{\xi_f}{a}\right)^{\alpha_\theta}\left[\left(\frac{r_{\text{up }1}}{r_0}\right)^{\alpha_1} - \left(\frac{r_{\text{low }1}}{r_0}\right)^{\alpha_1}\right], \qquad I_2 \equiv \frac{2}{3\alpha_2}\left(\frac{2\xi_f}{3}\right)^{\alpha_\theta}\left[\left(\frac{r_{\text{up }2}}{r_0}\right)^{\alpha_2} - \left(\frac{r_{\text{up }2}}{r_0}\right)^{\alpha_2}\right],$$

where

$$\alpha_1 \equiv 3 + \alpha_r - \alpha_\theta/2 + 3\alpha_\omega/2 - n\alpha_\theta/m , \qquad \alpha_2 \equiv \alpha_1 - n\alpha_\theta/m ,$$

$$r_{\text{up }1} \equiv \min(r_{\max}, r_{\omega t}, r_{\omega\max}, r_{\theta*\min 1}) , \qquad r_{\text{up }2} \equiv \min(r_{\max}, r_{\omega\max}, r_{\theta*\min 2}) ,$$

$$r_{\text{low }1} \equiv \max(r_{\min}, r_{\omega\min}, r_{\theta*\max 1}) , \qquad r_{\text{low }2} \equiv \max(r_{\min}, r_{\omega\min}, r_{\omega t}, r_{\theta*\max 2}) ,$$

$$r_{\omega\text{ ext}} \equiv [(\omega/\omega_p)_{\text{ext}}/(\omega/\omega_0)]^{2/3} r_0 , \qquad r_{\theta*\text{ ext }1} \equiv (\xi_f/\theta^m{}_{\text{ext}})^{2/(m+n)} r_0 , \qquad r_{\theta*\text{ ext }2} \equiv (\tfrac{4}{9})(\xi_f/\theta_{*\text{ ext}})^2 r_0 ,$$

and the subscript "ext" stands for "max" or "min," used consistently in the last three expressions. Figure 6 graphically illustrates these radii in the (r, θ_0)-plane. Calculating the flux in the X-mode is identical to the low-density O-mode calculation (so that $r_{\omega t}$ should be replaced by $r_{\min}$).

Two particular limiting cases are of interest: (i) broad-band emission in frequency in a narrow range of radius and (ii) narrow-band emission over an extended range in radius.

1. *Broad-band emission in frequency, narrow range in radius.*—At low frequencies $r_{\text{up }1} = r_{\max} = r_0 + \Delta r$, $r_{\text{low }1} = r_{\min} = r_0$ and the second integral in equation (51) can be ignored, while at high frequencies, $r_{\text{low }2} = r_{\min} = r_0$, $r_{\text{up }2} = r_{\max} = r_0 + \Delta r$ and the first integral is zero so that equation (51) becomes

$$F_\omega(\xi_f, \eta_f, d) = \begin{cases} \frac{2}{3}\left(\frac{2u_-}{u_+}\right)\frac{j_0 r_0^2 \Delta r}{d^2}\left(\frac{\omega}{\omega_0}\right)^{\alpha_\omega}\left(\frac{\xi_f}{a}\right)^{\alpha_\theta/m}\frac{1}{\theta_{*\max}^{\alpha_\theta}} & \omega < \omega_{\text{br}} , \\ & a\theta_{*\min}^m < \xi_f < a\theta_{*\max}^m \\ \frac{4}{9}\frac{j_0 r_0^2 \Delta r}{d^2}\left(\frac{2\xi_f}{3\theta_{*\max}}\right)^{\alpha_\theta} & \omega > \omega_{\text{br}} , \\ & 3\theta_{*\min}/2 < \xi_f < 3\theta_{*\max}/2 \\ 0 & \text{otherwise} \end{cases} . \tag{52}$$

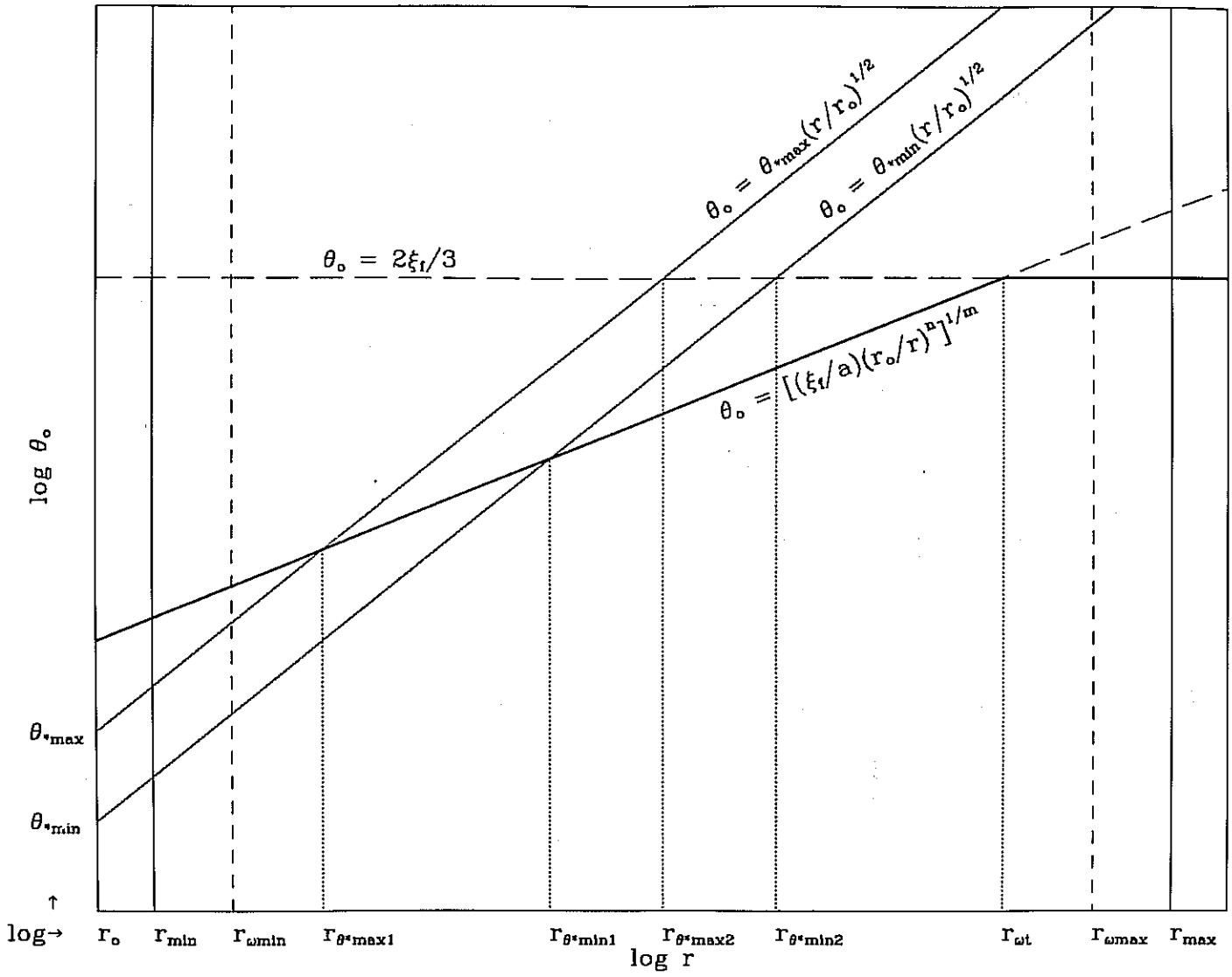

FIG. 6.—Integration of emissivity in log r – log θ_0 plane. A schematic representation of the integration plane in eq. (45) (after integration over ϕ_0). Here $m = -0.721$, $n = -0.210$, $a = 1.66\alpha_0^{0.07}$. Each integration occurs with ξ_f and ω held constant, with $\theta_{*max(min)}$, $r_{max(min)}$, and $(\omega/\omega_p)_{max(min)}$ constant parameters, depending on the density model and emission mechanism. Heavy dark line indicates the only points where the δ-function in eq. (46) is nonzero, and the limits yield a contribution only between $r_{\theta *max\,1}$ and $r_{\theta *min\,1}$ for this particular choice of parameters.

In this case the pulse width as a function of frequency reflects the frequency dependence of equations (39) and (40), whereas the dependence of the flux on frequency is determined solely by the frequency dependence of the emission mechanism (i.e., through α_ω).

2. *Narrow-band emission in frequency, large range in radius.*—Here use of the first or second term in equation (51) depends on what is taken to be the narrow emission band. RS and Cheng and Ruderman (1979) assume emission occurs when $\omega \approx ck$ and $\omega' \approx \omega'_p$, which requires $\alpha^{1/2} \approx 1/(2\gamma^2)$. This borders the regime between $p = \frac{1}{2}$ and $p = 1$, so the amount of refraction occurring depends on how broad band the emission is. For illustration we ignore refraction and let

$$(\omega/\omega_p)_{max} = (\omega/\omega_p)_c + (\Delta\omega/\omega_p)/2 \qquad \text{and} \qquad (\omega/\omega_p)_{min} = (\omega/\omega_p)_c - (\Delta\omega/\omega_p)/2,$$

with $(\Delta\omega/\omega_p) \ll (\omega/\omega_p)_c$. Then $r_{min} = r_{\omega\,min}$ and $r_{max} = r_{\omega\,max}$, and equation (51) becomes

$$F_\omega(\xi_f, \eta_f, d) = \begin{cases} \dfrac{8}{27}\dfrac{j_0 r_0^3}{d^2}\left(\dfrac{\omega}{\omega_0}\right)^{\alpha_\omega - 2\alpha_2/3}\left(\dfrac{\Delta\omega}{\omega_p}\right)\left(\dfrac{\omega}{\omega_p}\right)_c^{2\alpha_2/3}\left(\dfrac{\xi_f}{\theta_{*max}}\right)^{\alpha_\theta} & \left[\dfrac{(\omega/\omega_p)_c}{\omega/\omega_0}\right]^{1/3}\theta_{*min} < \xi_f < \left[\dfrac{(\omega/\omega_p)_c}{\omega/\omega_0}\right]^{1/3}\theta_{*max}\,, \\ 0 & \text{otherwise} \end{cases} \tag{53}$$

In this case the pulse width is $\sim\omega^{-1/3}$, and the spectrum is independent of the emission spectral index (since it is emitted in a small frequency band) but instead depends on the spatial emissivity parameters α_r and α_θ. If the emissivity is proportional to density, then $\alpha_\theta = 0$ and $\alpha_r = -3$, so that F_ω is constant in frequency (since the decrease in density at larger radii is compensated by increase in volume). The observed spectral index of ~ -1 to -2 must in this case come about from an emissivity which is proportional to a

lower power of density ($j_\omega \approx N^{1/2}$ or N^0 for $F_\omega \approx \omega^{-1}$ or ω^{-2}, respectively), or the emissivity must decrease rapidly with increasing θ_* ($\alpha_\theta \sim -3$ to -6) to account for the observed spectral index.

iii) *Polarization*

If propagation in the high-density regime occurs in both the *X*-mode and *O*-mode polarizations, the *O*-mode will be angularly separated by large angles ($\gtrsim$ subpulse widths). Thus the outflowing plasma acts like a polarizing beam splitter in the same way that was proposed by Melrose and Stoneham in the low-density limit. At high frequencies the *X*- and *O*-modes do not separate, and so the polarization reflects the polarization of the emission region.

The final polarization state of the radio radiation will be determined by the polarization state at the polarization limiting radius (PLR), i.e. the point where $\Delta k s \approx 1$ (Budden 1961; Melrose and Stoneham 1977; Cheng and Ruderman 1979; Stinebring *et al.* 1984*a*, *b*). Here Δk is the difference in wave vectors between the two polarization states for waves with the same frequency, and s is the scale length in the variation of the polarization parameters. An *O*-mode ray which is propagating toward the observer in direction n_f at the PLR will have a polarization angle ψ given by the angle between the projection of the magnetic field direction onto the sky b_s and some other fiducial direction such as the projection of the rotation axis onto the sky Ω_s:

$$\psi \equiv \angle(b_s, \Omega_s) = \angle\left[\frac{n_f \times (b \times n_f)}{|b \times n_f|}, \frac{n_f \times (\Omega \times n_f)}{|\Omega \times n_f|}\right], \tag{54}$$

so that

$$\tan \psi = \frac{|\Omega_s \times b_s|}{\Omega_s \cdot b_s} = \frac{[1 - (b \cdot \Omega)^2 - (n_f \cdot b)^2 - (n_f \cdot \Omega)^2 + 2(n_f \cdot b)(n_f \cdot \Omega)(\Omega \cdot b)]^{1/2}}{b \cdot \Omega - (n_f \cdot b)(n_f \cdot \Omega)} . \tag{55}$$

In equations (54) and (55) b is evaluated at the PLR, whereas n_f is evaluated at the RLR. (By assumption, n_f is also the direction of the ray at the PLR since refraction at altitudes higher than the RLR is neglible.) The *X*-mode position angle is displaced by $\pi/2$ from that given in equation (55). When a dipolar magnetic field is used for b, equation (55) becomes

$$\tan \psi \approx (3\theta_x/2 - \delta \sin i)/[3\theta_y/2 - (\alpha - i)] . \tag{56}$$

Here we have maintained only linear terms in the numerator and denominator. Also, θ_x and θ_y are defined in Appendix B, and δ, α, and i are the rotational phase angle, the angle between Ω and the line of sight (n_f), and the inclination angle between Ω and the magnetic moment μ, respectively (see Fig. 5). Note that equation (56) is only correct as long as the rotation of the pulsar can be neglected. For pulsar rotation periods less than $\sim$0.1 s rotational effects become important in determining the polarization angle (Barnard 1986).

For a ray which is emitted along the magnetic field direction, the magnetic azimuth of the ray is constant along the trajectory, and it is easy to show (e.g., Fawley 1978) that for each magnetic azimuth, ϕ_0, there is a unique rotational phase angle δ for the wave vector to be parallel to an observers direction which is given by

$$\tan \phi_0 = \theta_x/\theta_y = \delta \sin i/(\alpha - i) . \tag{57}$$

Substitution of equation (86) into equation (85) yields a polarization position angle of

$$\tan \psi = \delta \sin i/(\alpha - i) . \tag{58}$$

The final ray direction of a ray at longitude δ is

$$\xi_f = [(\alpha - i)^2 + \delta^2 \sin^2 \alpha]^{1/2} . \tag{59}$$

Equations (57)–(59) are the approximate expressions of the equations describing ϕ_0, ψ, ξ_f derived before (see, e.g., Fawley 1978, p. 39, or Manchester and Taylor 1977, p. 215) in the context of the Radhakrishnan and Cooke (1969; hereafter RC) magnetic pole model for the emission. So, given a particular orientation of rotation and magnetic axes and at a given pulse longitude, the polarization angle and emission direction are determined. For emission along the magnetic field, then, refraction only changes the initial value of ξ for a given ξ_f and thus δ, but does not change the polarization angle for a given δ.

Observations by Backer and Rankin (1980) and Stinebring (1982) indicate that at each pulse longitude there is a finite range in the position angle $\Delta\psi$. One contribution to this range is the fact that beaming is not a δ-function along the magnetic field but instead has a finite emission angle $\Delta\theta_b$. The quantity $\Delta\theta_b$ is commonly taken to be of order $1/\gamma$ as it is for single particle emission, but this may be a function of the plasma instability producing the coherence. Since finite $n_\perp$ at emission yields ray paths which are no longer confined to one magnetic azimuth, the position angle at a particular pulse longitude will reflect this range in beaming angle as a range in polarization angle and as a decrease in fractional linear polarization.

We may estimate this effect as follows. Differentiating equation (56), leaving δ constant, and evaluating at the PLR (indicated by subscript p) yields

$$\Delta\psi = \tfrac{3}{2} \cos^2 \psi[\Delta\theta_{xp} - \tan \psi \Delta\theta_{yp}]/[3\theta_{yp}/2 - (\alpha - i)] . \tag{60}$$

We wish to calculate $\Delta\theta_{xp}$ and $\Delta\theta_{yp}$ leaving the final ray directions (ξ_f, η_f) fixed but varying the initial direction and position of the ray (θ_{0x}, θ_{0y}, ξ_i, η_i) by amounts of order $\Delta\theta_b$. For simplicity we calculate $\Delta\psi$ at $\delta = 0$ ($\tan \psi = 0$) at which point $\theta_{0x} = 0$. Small displacements in the initial position and direction of a ray yield a change in the location of the RLR:

$$\Delta\theta_{xf} = \frac{\partial\theta_{xf}}{\partial\xi_i} \Delta\xi_i + \frac{\partial\theta_{xf}}{\partial\eta_i} \Delta\eta_i + \frac{\partial\theta_{xf}}{\partial\theta_{0x}} \Delta\theta_{0x} + \frac{\partial\theta_{xf}}{\partial\theta_{0y}} \Delta\theta_{0y} , \tag{61}$$

where all derivatives are taken at $\theta_{0x} = 0$, and at constant ξ_f and η_f. Calculation of the derivatives is involved and is outlined in Appendix D. The result is

$$\Delta\theta_{xf} = \frac{\theta_{yf}}{\theta_{0y}}\left[\frac{u_{xf}-1}{u_+ u_-}\right]\Delta\theta_{bx} \approx \begin{cases} -0.387(\theta_{yf}/\theta_{0y})\Delta\theta_{bx} & \omega < \omega_{\rm br} \\ -\frac{2}{3}\Delta\theta_{bx} & \omega > \omega_{\rm br} \end{cases}. \tag{62}$$

Here $\Delta\theta_{bx}$ is the angle between b and k in the (x-z)-plane. The direction of the ray is fixed at the RLR, but the polarization is fixed at the PLR. Use of equation (B8) shows that if the radius of the PLR is much greater than that of the RLR (but much less than the light cylinder radius), then

$$\theta_{yp} = (\tfrac{3}{2} - u_{yf})\theta_{yf} = \begin{cases} 1.08\theta_{yf} & \omega < \omega_{\rm br} \\ \frac{3}{2}\theta_{yf} & \omega > \omega_{\rm br} \end{cases}. \tag{63}$$

Ignoring factors of order unity equation (89) becomes

$$\Delta\psi \approx \frac{\Delta\theta_b}{\theta_{0y}} \approx \begin{cases} \xi_f^{-1.4}\alpha^{0.10}\Delta\theta_b & \omega < \omega_{\rm br} \\ \xi_f^{-1}\Delta\theta_b & \omega > \omega_{\rm br} \end{cases}. \tag{64}$$

If $\Delta\theta_b \approx 1/\gamma \approx 0.01$ and $\xi_f \approx 10°$, then $\Delta\psi \approx 5°$. At low frequency this can be several times greater. Refraction will broaden the dispersion in polarization angle with slightly steeper frequency dependence than it broadens the pulse width. The fractional polarization will be reduced slightly since the observer will sample a range in position angle. If the rays from different field lines add incoherently, the fractional polarization will be equal to $\int I(\Psi)\cos 2(\Psi - \Psi_0)d\Psi / \int I(\Psi)d\Psi \approx 1 - 2\Delta\Psi^2/3$, where Ψ_0 is the polarization angle when perfect beaming along field lines is assumed. Thus for $\Delta\Psi \approx 5°$ the fractional polarization is 99%, which is still quite high, and so is not a severe constraint.

b) Transverse Density Gradients

It is likely that the plasma density gradient in the open field zone of pulsars is not simply in the radial direction. Observationally, the occurrence of single and double pulses is consistent with a hollow cone of radiation (Backer 1976) which may also reflect the density of the emitting plasma. From a theoretical viewpoint, the pair plasma should fall off rapidly near the boundary of the open flux tube due to the smaller potential drop experienced by the pair-producing primary particles (AS). The presence of transverse gradients can greatly increase the angular deviation of a refracted ray. With inclusion of the transverse term the linearized equation (27) becomes

$$r\frac{dn_\perp}{dr} = \frac{3\theta_0 n_\parallel}{4} - \frac{3n_\perp}{2} - \frac{l\alpha}{pn_\parallel - q}\left(\frac{3\theta_0}{2} - \frac{\partial \ln N}{\partial\theta_0}\right). \tag{65}$$

If the transverse gradient scale is the width of the open flux tube, then the second term in parentheses in equation (65) is of order $1/\theta_0^2$ times the first term in parentheses. For $p = \frac{1}{2}$ the transverse term is of order $\alpha^{1/2}/\theta_0$ which, for the high-density fast mode, is much larger than any other term. Since $n_\perp$ changes more rapidly with radius than before, $\alpha^{1/2}$ can be larger when $n_\perp^2 \approx \alpha^{1/2}$. Further, if the density decreases in the direction away from the magnetic pole, $dn_\perp/dr$ is less than zero, so that $n_\perp$ can be negative when the wave decouples. The angle ξ_f is thus much larger than either the original angle of emission or that produced by a radial density gradient.

In terms of the phase velocity this is easily understood. Since $\beta_{\rm ph} \approx 1 + \alpha^{1/2}$ the fronts of constant phase move fastest near the center of the flux tube and slowest near the edge. Thus $n_\perp$ tends to decrease (although in absolute magnitude, it can be increasing). This is opposite to the effects of the curving field which tends to increase $n_\perp$.

To measure quantitatively the effects of the transverse gradients we have used an exponential distribution in θ_0:

$$N_{p0}(\theta_0) = N_{pc}\exp\left[-(\theta_0/\theta_w)^{n_w}\right]. \tag{66}$$

Here $N_{\rm pc}$ is the pair density at the center of the polar flux tube ($\theta_0 = 0$) and $r = r_0\theta_w$ and n_w are constant parameters of the distribution.

We have plotted the contours of constant density in Figure 7 for the distribution (66) using $\theta_w = 0.08$ and $n_w = 2$, along with the ray paths for several different frequencies, for two different initial colatitudes θ_0. As explained above, since the gradient points inward, k tends to point outward, with the group velocity in the direction halfway between $\boldsymbol{b}$ and $\boldsymbol{n}$. In Figure 8 we give examples of ξ_f versus frequency for several values of the initial colatitude θ_0, for the same parameters in equation (66). We note that $d\log\xi_f/d\log\omega$ varies from -0.14 when the ray is traversing essentially a radial gradient (see eq. [39]) to ~ -0.5 for those ray paths in which a steep transverse gradient is encountered when α is still large.

We may estimate $d\log\xi_f/d\log\omega$ for the case of a very strong transverse gradient. In that case, from equation (65) the scale length for growth of $n_\perp$ is on the order of $r\theta_N/\alpha^{1/2}$, where θ_N is the scale in θ_0 over which N_p varies substantially. This scale length can be much smaller than the radius r. But growth only occurs when the wave is coupled to the plasma, limiting $|n_\perp|$ to be $\sim 2^{1/2}\alpha_0^{1/4}$. The wave thus almost immediately decouples from the plasma, with a terminal ξ_f given by

$$\xi_f \approx 3\theta_0/2 + \sqrt{2}\,\alpha_0^{1/4}. \tag{67}$$

The corresponding break frequency occurs when the two terms on the right-hand side of equation (67) are set equal:

$$\omega_{\rm br} \approx 8\xi_f^{-2}\langle\gamma^{-3}\rangle^{1/2}. \tag{68}$$

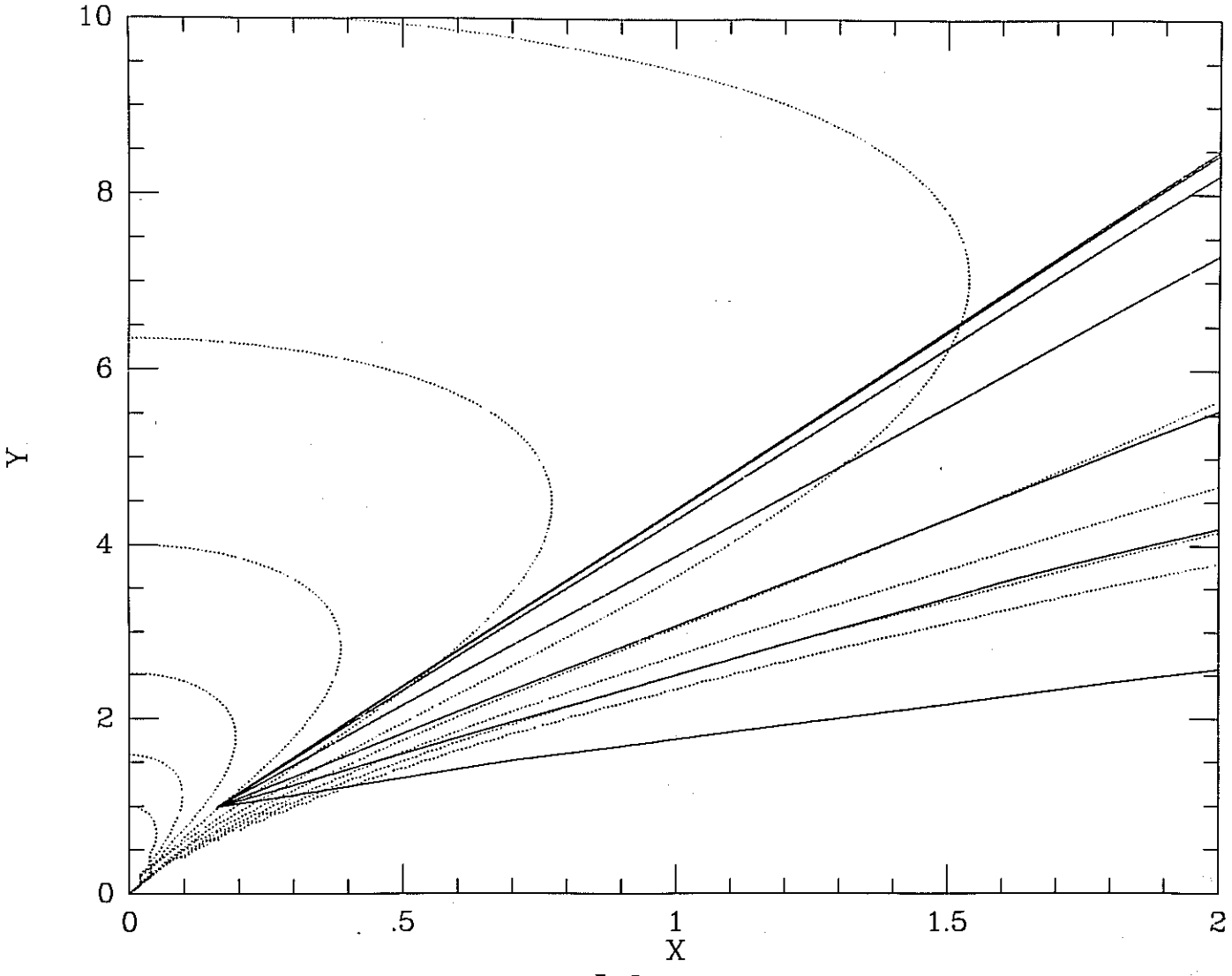

FIG. 7a

FIG. 7.—Ray paths through a transverse gradient. (*a*): Ray paths (*solid lines*) for seven different frequencies through the density distribution of eq. (66) with $\theta_w = 0.08$ rad, $n_w = 2$, $\gamma_0 = 100$ and $\theta_0 = 0.16$ rad. Each density contour (*dotted line*) shows density levels down by a factor of $\frac{1}{4}$. (*b*): Same as (*a*), but with $\theta_0 = 0.04$ rad.

We have plotted equation (67), along with the radial gradient result (39) and with the numerical results of a family of exponential density distributions with the same central density, and the same density at a common initial colatitude θ_0, but various θ_w's and n_w's in Figure 9, to illustrate the effects of increasing the transverse gradient. As can be seen, equation (67) accurately represents the low-frequency behavior of very strong transverse density gradients and provides an upper limit for most distributions at all frequencies.

It is apparent, however, that for the steepest gradients, at intermediate frequencies, further refraction can take place. This occurs because even though equation (67) is initially correct, the curving field lines reduce $n_\perp$ and also allow the rays to penetrate into large-density regions near the central field line ($\theta_0 = 0$), allowing the rays to recouple to the plasma. Since additional refraction can take place, equation (67) is an approximate upper limit to ξ_f.

IV. OBSERVATIONAL CONSEQUENCES

As indicated in § III the frequency dependence of intensity, pulse shape, and polarization will all be affected in a plasma where refractive effects are important. Some relevant observations include the following:

1. Malofeev and Malov (1980, hereafter MM) find that pulsar spectra are power laws between ν_m and ν_c with spectral index $\alpha_s = -1.96 \pm 0.57$. The quantity ν_m is the frequency of maximum intensity which MM find to be roughly correlated with rotation period, P, going approximately as $\nu_m \approx 10^8 P^{-0.5}$ Hz; ν_c is the frequency above which the spectrum is significantly steeper, and which MM find is also roughly correlated with period: $\nu_c \approx 2.9 \times 10^9 P^{-0.5}$ Hz.

2. The component separation and pulse widths of double components increase with decreasing frequency, with index $\alpha_w \approx -0.24 \pm 0.07$ (Sieber, Reinecke, and Wielebinski 1975). At high frequencies the separation is less dependent on frequency, $\alpha_w \approx 0. \pm 0.08$.

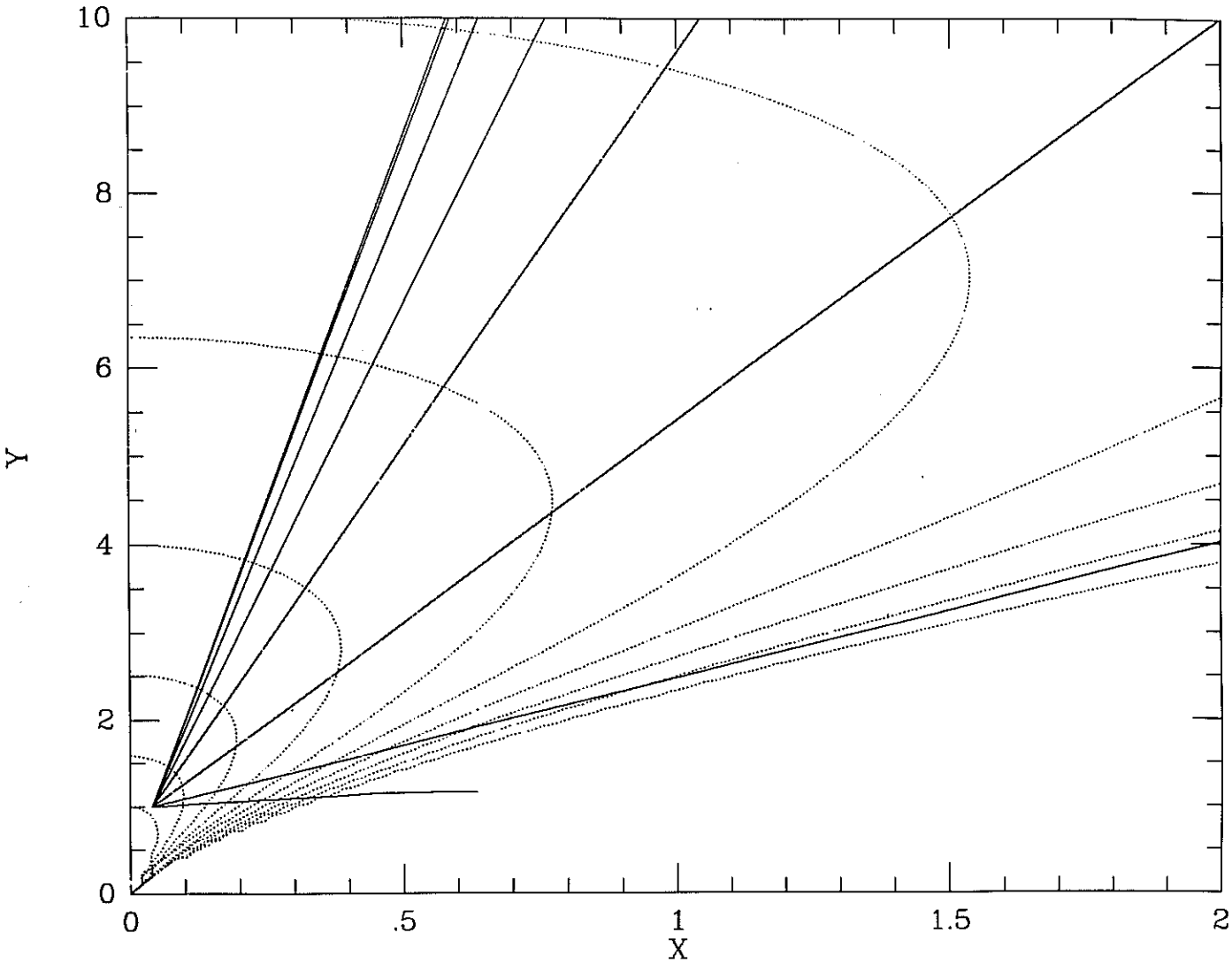

FIG. 7*b*

The frequency ν_w at which the high-frequency power law intersects the low-frequency power law was found by Sieber *et al.* to be correlated with ν_c. The tabulation of the parameters ν_m and ν_c by MM, however, seems to weaken the strength of the correlation found by Sieber *et al.* Rankin (1983*a*, *b*) finds that pulsars with single components (both "conal" and "core") tend to exhibit pulse widths which decrease with increasing frequency, except that at low frequency "absorption notches" are observed (i.e., pulse widths which are narrower than the extrapolation of the high-frequency pulse width vs. frequency curve, first observed by Bartel 1981.)

3. Radhakrishnan and Cooke (1969, hereafter RC) first proposed that the observed swing in polarization position angle is due to the rotation of the projection of the dipolar magnetic field (or field line curvature vector) onto the sky as the pulsar rotates. Manchester, Taylor, and Huguenin (1975), Backer, Rankin, and Campbell (1976), and Backer and Rankin (1980) have shown that in addition over a substantial fraction of the observed pulse, there is intensity at two polarization angles, displaced by 90°, each approximately obeying RC's continuous swing in position angle. Stinebring *et al.* (1984*a*, *b*) have extended Backer and Rankin's 430 MHz results to 800 and 1400 MHz to investigate the frequency dependence of the "orthogonal moding," and find qualitatively the same behavior at higher frequency.

As discussed in § III, the frequency dependence of pulse width and double pulse separation at low frequency has been explained before as a radius to frequency mapping (see RS or Komesaroff 1970) with the local plasma frequency decreasing with radius, thus giving larger pulse separations at lower frequencies. In this view the constancy of separation at $\nu > \nu_w$ is then associated with a minimum emission radius. The emission at frequencies above ν_w would then reflect the high-frequency tail of the emission mechanism at this radius. In contradiction to the basic assumptions of the radius to frequency mapping hypothesis, however, this requires the emission to be intrinsically broad band, with the plasma frequency appearing as a lower cutoff. Two consequences of this model are the following:

1. A correlation of ν_w with ν_c: as discussed earlier, Sieber, Reinecke, and Wielebinski (1975) find that ν_w is correlated with ν_c. However, when values of ν_c found by MM are used, the strength of the correlation is weakened.

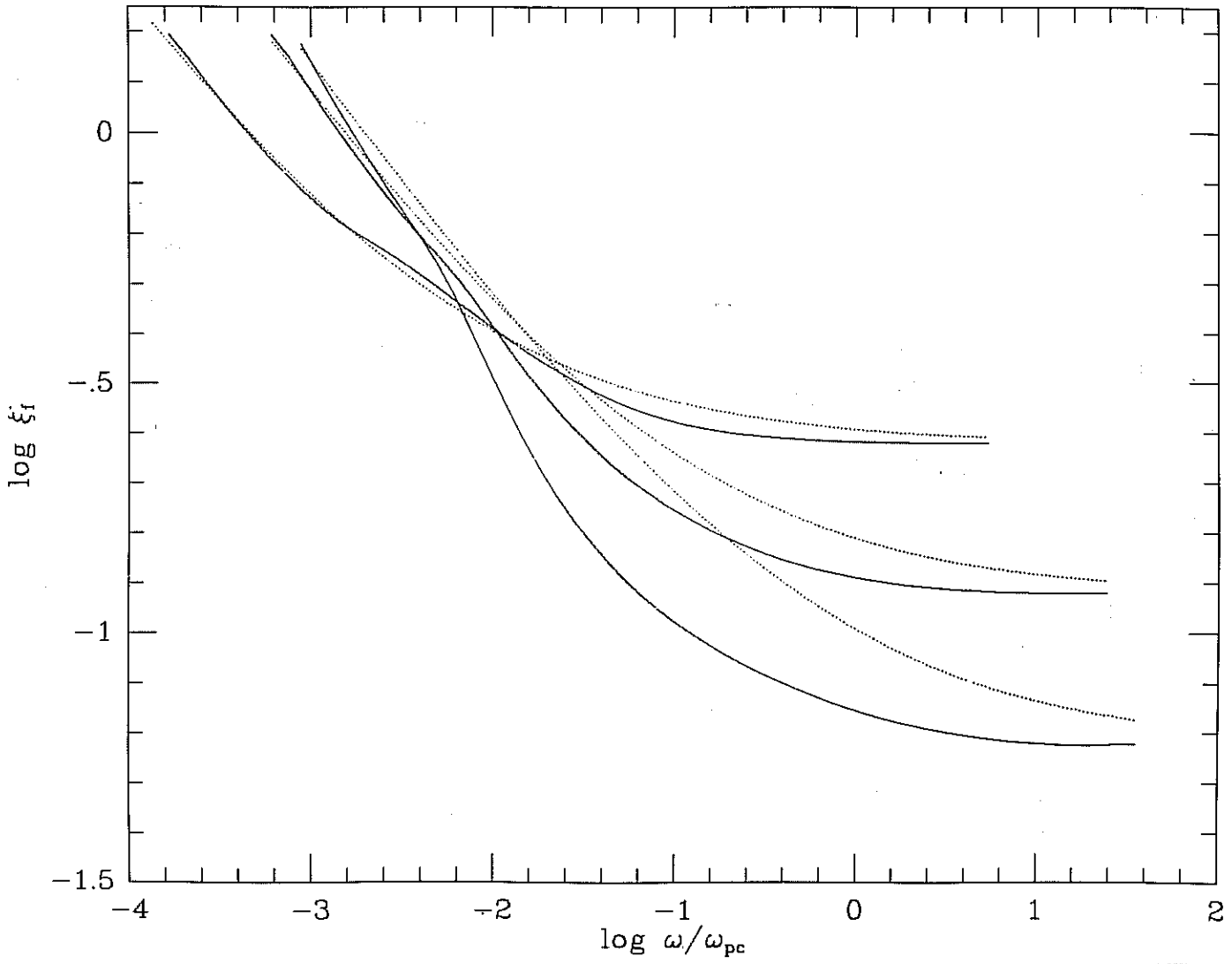

FIG. 8.—*Solid lines*: ξ_f vs. the frequency in units of the plasma frequency at $\theta_0 = 0$, and $r = r_0$, for $\theta_0 = 0.04$, 0.08, 0.16 for the same density parameters as Fig. 7. *Dotted lines*: the results using the extreme transverse gradient approximation (eq. [67]).

2. Frequency-dependent time delays, due to rotational aberration and longer path lengths at lower altitude (Cordes 1978): however, Cordes 1978 has found no displacement in the centroids of double component pulsars. Within the context of the radius to frequency mapping model, this requires the emission radius to be less than $\sim 10^8$ cm. Rickett and Cordes (1980) used micropulses as fiducial points and claimed to observe a time delay yielding emission radii of $\sim 10^7$ cm in PSR 0950+08, although the absence of micropulse widening with decreasing frequency raises questions of the validity of using micropulses as fiducial points. The most striking argument against radius to frequency mapping, though, occurs in the millisecond pulsar 1937+214. Cordes and Stinebring (1984) find that the time delay not accounted for by interstellar dispersion and scattering between pulses at 0.32 and 1.39 GHz is at most ± 6 μs, corresponding to a change in radius of ± 2 km, which is much less than 1 stellar radius or the expected radial change of ~ 30 km if radiation at high frequency occurs all the way down at the stellar surface. Since the frequency dependence of pulse width is typical for PSR 1937+214 ($\alpha_w \approx -0.38$), the absence of refraction when time delays for this and other pulsars argues against the canonical radius to frequency mapping.

An alternative explanation is that broad-band emission occurs in a narrow range in radius, but that refraction broadens low-frequency pulses. The high-frequency flattening of pulse separation with frequency is then accounted for by the absence of refraction when ω exceeds ω_{br} (see eqs. [40] and [68]). We may test this hypothesis in the context of pair-creation polar cap models by comparing the observed break frequency in double-pulse component separation θ_s with that given by equation (40) or (68). Pair creation models yield pair densities N at the emission radius r_e of

$$N = \frac{\kappa \Omega B_s \cos i}{2\pi c e} \left(\frac{r_e}{R}\right)^{-3} . \tag{69}$$

Here κ is the number of pairs formed per primary particle: $\sim 10^3$–10^5. The surface field strength, assuming braking due to magnetic

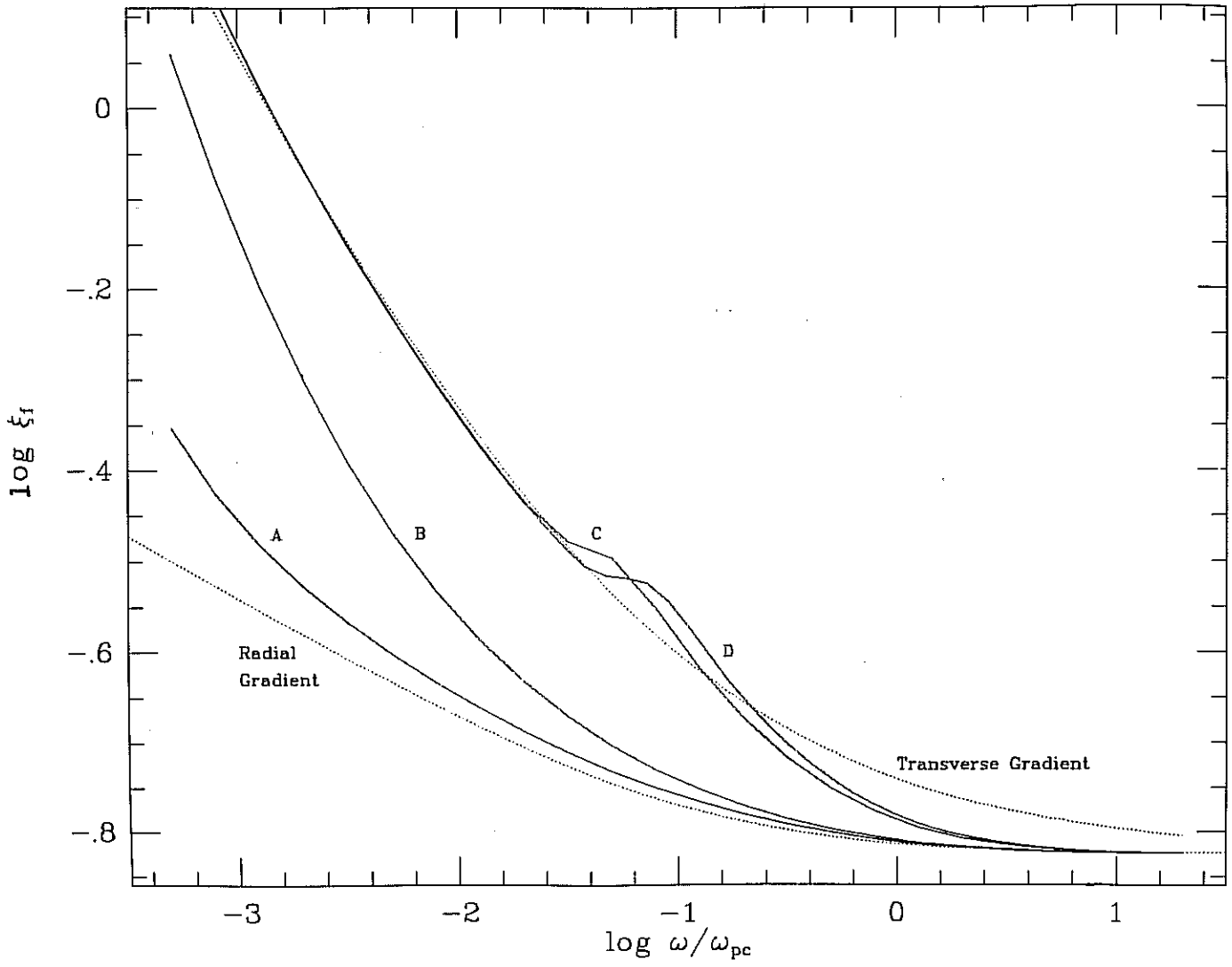

FIG. 9.—log ξ_f vs. log ω/ω_{pc} for a family of density distributions (eq. [66]) having constant central density and constant density at θ_0, but with steepening gradient, progressing from A to D. Parameters are A, $\theta_w = 0.0001$, $n_w = 0.047$; B, $\theta_w = 0.05$, $n_w = 0.47$; C, $\theta_w = 0.095$, $n_w = 6.37$; D, $\theta_w = 0.096$, $n_w = 8.00$. *Dotted lines*: the radial density gradient result (eq. [39]) and the extreme transverse gradient (eq. [67]) result are shown.

dipole radiation, is given by Ostriker and Gunn (1969):

$$B_s \approx 1.0 \times 10^{12}(P\dot{P}_{-15})^{1/2}/\sin i \,. \tag{70}$$

Here $\dot{P}_{-15} \equiv \dot{P}/10^{-15}$ ss^{-1}, and P is measured in seconds.

We assume the field lines on which the emission is maximum intercept the surface at some colatitude θ_* that is a fraction f_{pc} of the Goldreich-Julian (1969) polar cap opening angle,

$$\theta_* = f_{pc}(R\Omega/c)^{1/2} = 0.^\circ 83 f_{pc} P^{-1/2} \,. \tag{71}$$

Since $\theta_s/2 \approx \xi_f \approx 3\theta_0/2$, r_e is given by

$$r_e/R = 530 P\theta_s^2/f_{pc}^2 \,. \tag{72}$$

Combining equations (40) and (69)–(73) yields

$$\nu_{w9} = 1.0\chi\theta_{s10}^{-5} P^{-7/4}\dot{P}_{-15}^{1/4} \,. \tag{73}$$

Here $\chi \equiv (\kappa_3 f_{pc}^6 \langle\gamma^{-3}\rangle_{-6}/\tan i)^{1/2}$, $\nu_{w9} \equiv \nu_w/10^9$ Hz, $\kappa_3 \equiv \kappa/10^3$, $\langle\gamma^{-3}\rangle_{-6} \equiv \langle\gamma^{-3}\rangle/10^{-6}$, and $\theta_{s10} \equiv \theta_s/10^\circ$.

In equation (73), χ is not directly observable but should be of order unity for pair creation models, and so we see that $\nu_w \approx 1$ GHz. We tabulate χ and $f_{pc}^2 r_e/R$ in Table 2, using the observed values of θ_s, ν_w, P, and $\dot{P}$ for six of the nine pulsars tabulated in Table 5 of Sieber, Reinecke, and Wielebinski 1975. (PSR 0834+06 and PSR 1919+21 were not used because of the apparent "absorption notches" in their pulse forms. The component-separation spectra of PSR 1929+10 was fitted by Sieber *et al.* by only one power law,

TABLE 2

COMPARISON OF OBSERVED AND CALCULATED BREAK FREQUENCY IN PULSE COMPONENT SEPARATION VERSUS FREQUENCY RELATION

PULSAR (PSR)	OBSERVED PARAMETERS						INFERRED PARAMETERS		
	α_w	ν_{w9}	ν_{m9}	θ_{s10}	P	$\dot{P}_{-15}$	χ	ν_{cut9}	$f_{pc}^2 r_e/R$
0329+54.....	−0.18	1.1	0.24	0.95	0.71	2.1	0.39	0.002	10.3
0525+21.....	−0.21	1.39	0.09	1.19	3.74	40.1	13.26	0.020	84.7
1133+16.....	−0.26	0.97	0.06	0.53	1.19	3.7	0.04	0.0004	5.3
1237+25.....	−0.18	1.41	0.11	0.90	1.38	0.95	1.48	0.001	17.9
2020+28.....	−0.20	0.96	0.20	0.93	0.34	1.9	0.09	0.001	4.7
2045−16.....	−0.15	1.5	<0.40	1.01	1.96	11.0	2.81	0.002	32.0

NOTE.—Here α_w is the low-frequency power-law index, $\nu_{w9} = \nu_w/10^9$ Hz, $\nu_{m9} = \nu_m/10^9$ Hz, $\theta_{s10} = \theta_s/10^\circ$, P is the period in seconds, $\dot{P}_{-15} = \dot{P}/10^{-15}$ ss^{-1}, $\nu_{cut9} = \nu_{cut}/10^9$ Hz, and χ is given by

$$\chi \equiv (\kappa_3 f_{pc}^6 \langle\gamma^{-3}\rangle_{-6}/\tan i)^{1/2} = 1.0 \nu_{w9} \theta_{s10}^5 P^{7/4} \dot{P}_{-15}^{-1/4},$$

with $\kappa_3 = \kappa/10^3$ and $\langle\gamma^{-3}\rangle_{-6} = \langle\gamma^{-3}\rangle/10^{-6}$. The quantities α_w, ν_{w9}, and θ_{s10} are from Sieber, Reinecke, and Wielebinski 1975, P and $\dot{P}_{-15}$ are from Manchester and Taylor 1977, ν_{m9} is from MM, χ is calculated as above (see eq. [73]), ν_{cut9} is from eq. (73), and $f_{pc}^2 r_e/R$ is from eq. (72).

although the data also appear consistent with $\nu_w \sim 1$ GHz.) The table indicates that χ is roughly of order unity, demonstrating rough consistency of observations with pair-production models and broad-band, single-altitude emission, and also more generally the apparent relevance of refraction in the high-density regime.

Also listed in Table 2 are the low-frequency turnover in pulsar spectra ν_m from MM. These must be greater than the propagation frequencies at the emission altitude. From equation (58) of Paper I, we have

$$\nu_{cut\,9} = 1.6 \times 10^{-3} \theta_{s10}^2 \nu_{w9} . \tag{74}$$

Here $\nu_{cut\,9} = (\omega_{cutoff}/2\pi)/10^9$ Hz. Since ν_m is typically a few times 10–100 MHz, whereas equation (74) predicts $\nu_{cutoff} \approx 1$ MHz, we again have rough consistency of this model with observations.

We also point out that in Table 2 the observed low-frequency power-law index varies from −0.15 to −0.26, which should be compared to indices of −0.14 to −0.50 for density gradient profiles which are purely radial to extremely transverse; this is in substantially better agreement with the observations than the single index −0.33 predicted by the simple radius to frequency map. Radius to frequency maps in plasmas flowing out along polar field lines more complex than dipolar have steeper indices (Barnard and Arons 1982), which worsens agreement between this narrow-band emission model and the data.

Frequency-dependent time delays would still occur, however, due to the different propagation times through the dispersive medium. Integration of equation (25) indicates that two different frequencies propagating through a purely radial density gradient will suffer a time delay Δt of

$$\Delta t \approx (\Delta\alpha_0^{1/2})(r_0/c) . \tag{75}$$

Here $\Delta\alpha_0^{1/2}$ is the difference in $\alpha_0^{1/2}$ for the two different frequencies.

In a strong transverse gradient the time lag is approximately that given in equation (75), with r_0 replaced by $\alpha_0/\nabla\alpha_0$, which can be much less than r_0. The frequency dependence of Δt is $\propto \Delta\omega^{-1}$ here, whereas for rotational effects it is $\propto \Delta\omega^{-2/3}$. Also low-frequency waves are observed first with rotational time delays, whereas low-frequency waves are observed last if propagation through the medium is the origin of the delay. (Field line sweep-back near the light cylinder, however, may also cause the low-frequency waves to be observed last in the radius to frequency model.) Since $\Delta\alpha_0^{1/2}$ is at *most* unity in the broad-band model, consistency with observations of PSR 1937+214 requires gradient scales less than $\sim$2 km. This may be consistent with dynamical models (see Arons 1983*a*).

It should also be pointed out that transverse density gradients may also produce frequency-dependent pulse widths even if all emission occurs beyond ω_{br}, if the local density is associated with a local frequency. A specific model would be required to determine whether refraction or the emission itself dominates in producing the frequency dependence of pulse widths.

As pointed out by Melrose and Stoneham (1977) and Melrose (1979), refraction is a candidate for the formation of orthogonal modes. The occurrence of regions in longitude similar to subpulse widths in which an orthogonal mode is preferred suggests angular deviations of several degrees. This is larger than can easily be accounted for in the low-density limit, but does occur at high density.

Stinebring *et al.* (1984*a*, *b*) ruled out refraction to account for the production of orthogonal modes by appealing to the rough frequency independence of the orthogonal moding. In four of nine pulsars studied, the orthogonal modes covered approximately the same range in pulse longitude, while four of nine had a greater extent at 430 MHz than 1404 MHz. However, they asumed that all the refraction occurs in the low-density limit ($n_\perp \gg \alpha_0^{1/4}$), while we have shown that so long as emission into the O-mode occurs with $n_\perp < \alpha_0^{1/4}$, the frequency dependence of the beam splitting is in much better accord with the observed production of orthogonal modes. In addition, if the emission process produces both X-mode and O-mode photons, the emergent polarization state depends on the relative intensity of the two modes, so long as the beam splitting is incomplete. Because the X-polarization is refracted very little, it would be expected to occur within a fixed pulse longitude range, restricted to relatively central pulse longitudes. Since the polarization state will be determined by which mode is more intense, the position within the range will vary depending on the ratio of X- to O-mode radiation, as well as on the frequency dependence of the refractive index. In any case, at frequencies above ω_{br} the

polarization state will not be affected by refraction, and any frequency dependence will be that due to the emission region. Since $\omega_{\rm br} \propto \theta^{-2}$, polarization flips can occur at frequencies substantially higher than ν_w.

V. CONCLUSION

We have investigated the propagation of waves in an outflowing electron-positron plasma and examined trajectories of waves through this plasma in three regimes: the Alfvén mode, high-density fast mode, and low-density fast mode (corresponding to $\sigma = 0$, $\frac{1}{2}$, and 1, respectively). If the emission mechanism generates Alfvén waves, the waves propagate outward along the field lines until the phase velocity of the waves is of the order of the particle velocities where Landau growth or damping occurs. Propagation to infinity requires coupling to the fast branch. If this coupling occurs at the comoving plasma frequency, pulse widths should vary as $\omega^{-1/3}$. In the $\sigma = \frac{1}{2}$ regime, wave trajectories are still bent by the curving field, but upon generation of sufficient $n_\perp$ they decouple and follow straight rays. For emission on the fast branch in a narrow range in radii and if the plasma density is uniform in magnetic colatitude, pulse widths vary as $\omega^{-0.14}$. If there are steep density gradients in θ_*, the pulse widths can vary as rapidly as $\omega^{-1/2}$. The dispersion in polarization position angle should have slightly steeper frequency dependence than pulse width. At high frequencies in the linear regime rays are straight, so that $\xi_f \propto \omega^0$ if emission occurs at one radius, but $\xi_f \approx \omega^{-1/3}$ if extended over radius (radius to frequency mapping). Refraction, however, can account for the high-frequency portion $\xi_f =$ constant and the low-frequency portion $\xi_f \approx \omega^{-1/5}$–$\omega^{-1/2}$ observed in pulsars if emission is broad band at one radius, without the problem of the observed absence of rotational time delays predicted by the radius to frequency hypothesis. *O*-mode transitions then are understood to be the result of angular separation of *X*- and *O*-mode waves. The observed frequency dependence of orthogonal moding is crudely consistent with this hypothesis. In contrast, the ω^{-2} variation of angular separation between the modes expected in the low-density regime *is* in conflict with the observations (Stinebring *et al.* 1984*a*, *b*). Because the angular separation and fractional polarization of the modes varies slowly in our model, observations over a wider range of frequency and nonaxisymmetric modeling are needed to test our theory. The decrease in fractional polarization at high frequency observed in the average pulsar waveforms is consistent with the merging of the two beams. However, the observations that individual subpulses are highly but not completely polarized argues for some type of intrinsic partial polarization of the emission process.

We have only considered a few possible emission scenarios in our treatment of wave propagation through the magnetosphere. The results are suggestive of important consequences for interpretation of pulsar radio data. The general ray tracing and radiative transfer equations developed in this work should prove to be useful in future work which predicts more precise magnetospheric conditions and emission mechanisms.

Helpful conversations with D. Backer, A. Konigl, and S. Kulkarni are gratefully acknowledged.

Our research on this topic was supported by NSF grants AST 79-23243, AST 82-15456, and AST 83-17462, by grant number 85-6 from the Institute of Geophysics and Planetary Physics, and by the taxpayers of California.

APPENDIX A

EVALUATION OF EXPRESSIONS IN EQUATIONS (6) AND (7)

Using the dispersion relations and equations (48) and (55) of Paper I, we find

$$\sum_s \omega_s^2 \frac{\partial g_s}{\partial n_\parallel} = \begin{cases} \dfrac{2\beta_0 \omega_p^2}{\gamma_0^3 (1-\beta_0 n_\parallel)^2} & \text{“cold” plasma} \\ \omega_p^2 g[h(\beta_{\max}, n_\parallel) + h(\beta_{\min}, n_\parallel)] & \text{waterbag} \end{cases}, \tag{A1}$$

$$\sum_s \frac{\partial \omega_s^2}{\partial x} = \begin{cases} \dfrac{1}{\gamma_0^3 (1-\beta_0 n_\parallel)^2} \dfrac{\partial \omega_p^2}{\partial x} & \text{“cold” plasma} \\ g \dfrac{\partial \omega_p^2}{\partial x} & \text{waterbag} \end{cases}, \tag{A2}$$

$$\sum_s \left.\frac{\partial g_s}{\partial x}\right|_{n_\parallel} \omega_s^2 = \begin{cases} \dfrac{\omega_p^2}{\gamma_0^3 (1-\beta_0 n_\parallel)^2} \left[\dfrac{-3}{\gamma_0} + \dfrac{2 n_\parallel}{\beta_0 \gamma_0^3 (1-\beta_0 n_\parallel)}\right] \dfrac{\partial \gamma_0}{\partial x} & \text{“cold” plasma} \\ g\omega_p^2 \left[\dfrac{1}{u_{\max} - u_{\min}} \left(\dfrac{1}{\beta_{\min}} \dfrac{\partial \gamma_{\min}}{\partial x} - \dfrac{1}{\beta_{\max}} \dfrac{\partial \gamma_{\max}}{\partial x}\right)\right. & \\ \left. + \dfrac{1}{h(\beta_{\max}, n_\parallel) - h(\beta_{\min}, n_\parallel)} \left[\dfrac{h^2(\beta_{\max}, n_\parallel)}{u_{\max}^3} \dfrac{\partial \gamma_{\max}}{\partial x} - \dfrac{h^2(\beta_{\min}, n_\parallel)}{u_{\min}^3} \dfrac{\partial \gamma_{\min}}{\partial x}\right] \right] & \text{waterbag} \end{cases}, \tag{A3}$$

Here g is given by equation (55) of Paper I, $h(\beta, n_\parallel) \equiv \beta/(1 - \beta n_\parallel)$, and $u_{\max(\min)} = \gamma_{\max(\min)} \beta_{\max(\min)}$.

APPENDIX B

RAY EQUATIONS IN THREE DIMENSIONS

Equations (11) and (12) are the ray equations for a cold $e^{\pm}$ plasma in the limit $\omega_c'/\omega_p' \gg 1$. The components of the unit vector along the magnetic field b are given through second order in x/z and y/z by

$$b_x = (\tfrac{3}{2})x/z\,, \qquad b_y = (\tfrac{3}{2})y/z\,, \qquad b_z = 1 - (\tfrac{9}{8})(x^2 + y^2)/z^2\,. \tag{B1}$$

Thus, through first order in x/z and y/z the gradient of b is given by

$$\frac{\partial b}{\partial x} = \left(\frac{3}{2z}\right)\begin{bmatrix} 1 & 0 & -\dfrac{3x}{2z} \\ 0 & 1 & -\dfrac{3y}{2z} \\ -\dfrac{x}{z} & -\dfrac{y}{z} & 0 \end{bmatrix}. \tag{B2}$$

If the density is uniform in θ_* but falls off with altitude as r^{-3}, then

$$l\alpha \frac{\partial \ln N}{\partial x_i} = -\frac{3l\alpha x_i}{r^2}\,. \tag{B3}$$

Here $x_i = x$, y, or z. For the Alfvén mode and low-density fast mode $l\alpha$ is only second order. For the high-density fast mode $l\alpha = \alpha^{1/2}/2$, yielding a second-order quantity when $x_i = x$ or y.

Thus, through first order, the six ray equations become

$$\begin{aligned} \frac{1}{c}\frac{dx}{dt} &= pn_x - \frac{3}{2}q\left(\frac{x}{z}\right), & \frac{1}{c}\frac{dn_x}{dt} &= q\left[\frac{3n_x}{2z} - \frac{9}{4z}\left(\frac{x}{z}\right)\right], \\ \frac{1}{c}\frac{dy}{dt} &= pn_y - \frac{3}{2}q\left(\frac{y}{z}\right), & \frac{1}{c}\frac{dn_y}{dt} &= q\left[\frac{3n_y}{2z} - \frac{9}{4z}\left(\frac{x}{z}\right)\right], \\ \frac{1}{c}\frac{dz}{dt} &= pn_z - q\,, & \frac{1}{c}\frac{dn_z}{dt} &= \frac{3l\alpha}{z}\,. \end{aligned} \tag{B4}$$

We define

$$\theta_x \equiv x/z\,, \qquad \theta_y \equiv y/z\,, \qquad n_{\perp x} \equiv \theta_x - n_x\,, \qquad n_{\perp y} \equiv \theta_y - n_y\,. \tag{B5}$$

Eliminating the time dependence and setting $p - q = 1$, we have

$$\frac{d\theta_i}{dz} = \frac{1}{z}\left(\frac{\theta_i}{2} - pn_{\perp i}\right), \qquad \frac{dn_{\perp i}}{dz} = \frac{1}{z}\left(\frac{3\theta_i}{4} - \frac{3}{2}n_{\perp i}\right). \tag{B6}$$

Here i takes on the values x or y. The equations, then, for each Cartesian component are the same as those for the rays when restricted to an azimuthal plane (see eqs. [29] and [30]).

The solution is again parametric (with parameters u_x and u_y):

$$\frac{\theta_x}{\theta_{0x}} = \left(\frac{u_{0x} - u_+}{u_x - u_+}\right)^{(1+a)/2}\left(\frac{u_{0x} - u_-}{u_x - u_-}\right)^{(1-a)/2}, \tag{B7}$$

$$\frac{\theta_y}{\theta_{0y}} = \left(\frac{u_{0y} - u_+}{u_y - u_+}\right)^{(1+a)/2}\left(\frac{u_{0y} - u_-}{u_y - u_-}\right)^{(1-a)/2}, \tag{B8}$$

$$\frac{z}{z_0} = \left(\frac{u_{0x} - u_+}{u_x - u_+}\right)^{-a}\left(\frac{u_{0x} - u_-}{u_x - u_-}\right)^{a} = \left(\frac{u_{0y} - u_+}{u_y - u_+}\right)^{-a}\left(\frac{u_{0y} - u_-}{u_y - u_-}\right)^{a}, \tag{B9}$$

$$n_{\perp x} = u_x\theta_x\,, \tag{B10}$$

$$n_{\perp y} = u_y\theta_y\,. \tag{B11}$$

Here $u_{0x} = n_{\perp 0x}/\theta_{0x}$, $u_{0y} = n_{\perp 0y}/\theta_{0y}$, $u_\pm = (1 \pm \frac{1}{2}a)/p$, and $a = 1/(4 - 3p)^{1/2}$. Since the parameters u_x and u_y must give the same value of z for a ray trajectory, equation (B9) yields

$$u_y = \frac{u_x(u_+ U_x - u_- U_y) + u_+ u_-(U_y - U_x)}{u_x(U_x - U_y) + u_+ U_y - u_- U_x}\,. \tag{B12}$$

Here $U_x = (u_{0x} - u_+)/(u_{0x} - u_-)$ and $U_y = (u_{0y} - u_+)/(u_{0y} - u_-)$.

The wave propagates outward in the high-density regime until the RLR where $n_\perp^2 \approx 2\alpha^{1/2}$, at which point further refraction is of order θ_0^2. Thus at the RLR $n_{\perp xf}^2 + n_{\perp yf}^2 \approx 2\alpha_0^{1/2}(z_0/z_f)^{3/2}$, so that

$$u_{xf}^2\theta_{xf}^2\left(\frac{u_{0x}-u_+}{u_{xf}-u_+}\right)^{(1+a)}\left(\frac{u_{0x}-u_-}{u_{xf}-u_-}\right)^{(1-a)} + u_{yf}^2\theta_{yf}^2\left(\frac{u_{0y}-u_+}{u_{yf}-u_+}\right)^{(1+a)}\left(\frac{u_{0y}-u_-}{u_{yf}-u_-}\right)^{(1-a)} - 2\alpha_0^{1/2}\left(\frac{u_{0x}-u_+}{u_{xf}-u_+}\right)^{3a/2}\left(\frac{u_{0x}-u_-}{u_{xf}-u_-}\right)^{-3a/2} = 0\,. \tag{B13}$$

Here α_0 is α evaluated at the emission point. Thus u_{xf} is given implicitly in equation (B13), from which any of the variables θ_{xf}, θ_{yf}, z_f, $n_{\perp xf}$, or $n_{\perp yf}$ can be found from equations (B7)–(B11).

APPENDIX C

EVALUATION OF $\left|\frac{\partial\Theta}{\partial\phi_0}\frac{\partial\Phi}{\partial\theta_0} - \frac{\partial\Theta}{\partial\theta_0}\frac{\partial\Phi}{\partial\phi_0}\right|$

In order to evaluate the integral in equation (45) we must evaluate the derivatives of $\Theta \equiv \xi_i - 3\theta_0/2$ and $\Phi \equiv \eta_i - \phi_0$ with respect to θ_0 and ϕ_0. Here ξ_i and η_i are regarded each as functions of ξ_f, η_f, θ_0, and ϕ_0, and the derivatives are evaluated with the three other variables held constant.

We have

$$\eta_i = \tan^{-1}\frac{(3/2 - p_0 u_{0x})\theta_{0x}}{(3/2 - p_0 u_{0y})\theta_{0y}}\,, \qquad \xi_i = [(\tfrac{3}{2} - p_0 u_{0x})^2\theta_{0x}^2 + (\tfrac{3}{2} - p_0 u_{0y})^2\theta_{0y}^2]^{1/2}\,, \tag{C1}$$

$$\eta_f = \tan^{-1}\frac{(3/2 - u_{xf})\theta_{xf}}{(3/2 - u_{yf})\theta_{xf}}\,, \qquad \xi_f = [(\tfrac{3}{2} - u_{xf})^2\theta_{xf}^2 + (\tfrac{3}{2} - u_{yf})^2\theta_{yf}^2]^{1/2}\,. \tag{C2}$$

Here p_0 is the parameter p evaluated at the emission point ($p_0 = \frac{1}{2}$ if $\alpha_0 > \frac{1}{4}\gamma_t^4$, and $p_0 = 1$ if $\alpha_0 < \frac{1}{4}\gamma_t^4$). Note that the direction (ξ, η) to the direction of the group velocity vector which at the RLR is in the $p = 1$ regime by definition.

We thus have η_i, ξ_i, θ_0, ϕ_0 as functions of θ_{0x}, θ_{0y}, u_{0x}, u_{0y}. Also, since u_{xf}, u_{yf}, θ_{xf}, and θ_{yf} are functions of the same variables, η_f and ξ_f can also be regarded as functions of θ_{0x}, θ_{0y}, u_{0x}, and u_{0y}.

Let

$$\boldsymbol{P} \equiv \begin{pmatrix} u_{0x} \\ u_{0y} \\ \Theta_{0x} \\ \Theta_{0y} \end{pmatrix} \qquad \text{and} \qquad \boldsymbol{F} \equiv \begin{pmatrix} \eta_f \\ \xi_f \\ \theta_0 \\ \phi_0 \end{pmatrix}. \tag{C3}$$

When the initial values $\boldsymbol{P}$ are incremented by an amount $\delta\boldsymbol{P}$, $\boldsymbol{F}$ changes by of an amount $\delta\boldsymbol{F}$, given by

$$\frac{\partial\boldsymbol{F}}{\partial\boldsymbol{P}}\cdot\delta\boldsymbol{P} \equiv \delta\boldsymbol{F}\,; \tag{C4}$$

here the ijth component of $\partial\boldsymbol{F}/\partial\boldsymbol{P}$ is given by $\partial F_i/\partial P_j$.

Define

$$\delta\boldsymbol{F}_1 \equiv \begin{pmatrix} 0 \\ 0 \\ 1 \\ 0 \end{pmatrix} \qquad \text{and} \qquad \delta\boldsymbol{F}_2 \equiv \begin{pmatrix} 0 \\ 0 \\ 0 \\ 1 \end{pmatrix} \tag{C5}$$

with corresponding $\delta\boldsymbol{P}_1$ and $\delta\boldsymbol{P}_2$ such that $(\partial\boldsymbol{F}/\partial\boldsymbol{P})\cdot\delta\boldsymbol{P}_1 \equiv \delta\boldsymbol{F}_1$ and $(\partial\boldsymbol{F}/\partial\boldsymbol{P})\cdot\delta\boldsymbol{P}_2 \equiv \delta\boldsymbol{F}_2$. Thus,

$$\delta\boldsymbol{P}_1 = \left(\frac{\partial\boldsymbol{F}}{\partial\boldsymbol{P}}\right)^{-1}\cdot\delta\boldsymbol{F}_1 \qquad \text{and} \qquad \delta\boldsymbol{P}_2 = \left(\frac{\partial\boldsymbol{F}}{\partial\boldsymbol{P}}\right)^{-1}\cdot\delta\boldsymbol{F}_2\,. \tag{C6}$$

From these definitions we obtain

$$\frac{\partial\eta_i}{\partial\phi_0}(\boldsymbol{F})\bigg|_{\theta_0,\eta_f,\xi_f} = \frac{\partial\eta_i}{\partial\boldsymbol{P}}(\boldsymbol{P})\cdot\delta\boldsymbol{P}_2\,, \tag{C7}$$

$$= \frac{\partial\eta_i}{\partial\boldsymbol{P}}(\boldsymbol{P})\left(\frac{\partial\boldsymbol{F}}{\partial\boldsymbol{P}}\right)^{-1}\cdot\delta\boldsymbol{F}_2\,, \tag{C8}$$

$$\frac{\partial\xi_i}{\partial\theta_0}(\boldsymbol{F})\bigg|_{\phi_0,\eta_f,\xi_f} = \frac{\partial\xi_i}{\partial\boldsymbol{P}}(\boldsymbol{P})\left(\frac{\partial\boldsymbol{F}}{\partial\boldsymbol{P}}\right)^{-1}\cdot\delta\boldsymbol{F}_1\,. \tag{C9}$$

Using the notation

$$[x, y]_{s,t} \equiv \left[\frac{\partial x}{\partial s}\frac{\partial y}{\partial t} - \frac{\partial x}{\partial t}\frac{\partial y}{\partial s}\right],$$

after inverting the matrix $\partial \boldsymbol{F}/\partial \boldsymbol{P}$ and performing the dot products in equation (C8) and (C9) we find

$$\frac{\partial \xi_i}{\partial \theta_0}(\eta_f, \xi_f, \theta_0, \phi_0) = \left\{\frac{[\xi_f, \phi_0]_{\theta_{0x}, \theta_{0y}}[\eta_f, \xi_i]_{u_{0y}, u_{0x}} + [\xi_f, \xi_i]_{u_{0x}, u_{0y}}[\eta_f, \phi_0]_{\theta_{0x}, \theta_{0y}}}{[\eta_f, \xi_f]_{u_{0x}, u_{0y}}[\theta_0, \phi_0]_{\theta_{0x}, \theta_{0y}}}\right\} + \frac{[\phi_0, \xi_i]_{\theta_{0y}, \theta_{0x}}}{[\theta_0, \phi_0]_{\theta_{0x}, \theta_{0y}}}, \tag{C10}$$

$$\frac{\partial \eta_i}{\partial \phi_0}(\eta_f, \xi_f, \theta_0, \phi_0) = \left\{\frac{[\eta_i, \xi_f]_{u_{0x}, u_{0y}}[\eta_f, \theta_0]_{\theta_{0x}, \theta_{0y}} + [\eta_i, \eta_f]_{u_{0y}, u_{0x}}[\xi_f, \theta_0]_{\theta_{0x}, \theta_{0y}}}{[\eta_f, \xi_f]_{u_{0x}, u_{0y}}[\theta_0, \phi_0]_{\theta_{0x}, \theta_{0y}}}\right\} + \frac{[\eta_i, \theta_0]_{\theta_{0x}, \theta_{0y}}}{[\theta_0, \phi_0]_{\theta_{0x}, \theta_{0y}}}. \tag{C11}$$

To proceed further we take advantage of the problem's symmetry.

$$\left.\frac{\partial \xi_i}{\partial \theta_0}\right|_{\xi_f, \eta_f} \quad \text{and} \quad \left.\frac{\partial \eta_i}{\partial \phi_0}\right|_{\xi_f, \eta_f}$$

are to be evaluated at $\xi_i = 3\theta_0/2$ and $\eta_i = \phi_0$. The result must be independent of ϕ_0. We may therefore evaluate the derivatives at a specific value of ϕ_0, but expect the result to hold for all ϕ_0. In particular, we let $\phi_0 = 0$. We also evaluate the derivatives at the values of ξ_f, η_f, θ_0, and ϕ_0 such that $\xi_i = 3\theta_0/2$ and $\eta_i = \phi_0$. This implies $u_{0x} = u_{0y} = \eta_i = \eta_f = 0$.

Many of the derivatives needed to evaluate equations (C10) and (C11) vanish because of the symmetry of the problem. They vanish for three general reasons:

1. The azimuthal variables (η_i, η_f, ϕ_0) are zero at the point where the derivatives are to be evaluated, and remain zero as long as the ray stays in the $\phi_0 = 0$ plane, which it does if $n_{\perp 0x}$ and θ_{0x} are zero. Thus derivatives of the azimuthal variables with respect to u_{0y} and θ_{0y} are zero:

$$\frac{\partial \eta_i}{\partial \theta_{0y}} = \frac{\partial \eta_f}{\partial \theta_{0y}} = \frac{\partial \phi_0}{\partial \theta_{0y}} = \frac{\partial \eta_i}{\partial u_{0y}} = \frac{\partial \eta_f}{\partial u_{0y}} = 0. \tag{C12}$$

2. The colatitude variables (θ_0, ξ_i, and ξ_f) will all be changed by incrementing the starting location of the ray out of the $\phi_0 = 0$ plane (i.e. by incrementing $\delta\theta_{0x}$). But because of the azimuthal symmetry the change in the colatitude variable will be the same for a positive increment in $\delta\theta_{0x}$ as it is for a negative increment in $\delta\theta_{0x}$. Thus, evaluated at $\theta_{0x} = 0$ the following must go to zero:

$$\frac{\partial \theta_0}{\partial \theta_{0x}} = \frac{\partial \xi_i}{\partial \theta_{0x}} = \frac{\partial \xi_f}{\partial \theta_{0x}} = 0. \tag{C13}$$

3. If X is one of the dependent variables that is a function of $\boldsymbol{P}$, then

$$\left.\frac{\partial X}{\partial u_{0x}}\right|_{\theta_{0x}, \theta_{0y}, u_{0y}} = \theta_{0x}\left.\frac{\partial X}{\partial n_{\perp 0x}}\right|_{\theta_{0x}, \theta_{0y}, u_{0y}}.$$

Since the derivatives of η_i, η_f, ξ_i, and ξ_f are all zero or finite, then evaluated at $\theta_{0x} = 0$,

$$\frac{\partial \xi_i}{\partial u_{0x}} = \frac{\partial \xi_f}{\partial u_{0x}} = \frac{\partial \eta_i}{\partial u_{0x}} = \frac{\partial \eta_f}{\partial u_{0x}} = 0. \tag{C14}$$

These zero derivatives allow substantial simplification of equations (C10) and (C11):

$$\left.\frac{\partial \xi_i}{\partial \theta_0}(\eta_f, \xi_f, \theta_0, \phi_0)\right|_{\xi_i = 3\theta_0/2, \eta_i = \phi_0 = 0} = \frac{\partial \xi_i}{\partial \theta_{0y}} - \left(\frac{\partial \xi_f}{\partial \theta_{0y}}\frac{\partial \xi_i}{\partial u_{0y}}\Big/\frac{\partial \xi_f}{\partial u_{0y}}\right), \tag{C15}$$

$$\left.\frac{\partial \eta_i}{\partial \phi_0}(\eta_f, \xi_f, \theta_0, \phi_0)\right|_{\xi_i = 3\theta_0/2, \eta_i = \phi_0 = 0} = \frac{\partial \eta_i}{\partial \theta_{0x}}\frac{\partial \phi_0}{\partial \theta_{0x}} - \left(\frac{\partial \eta_f}{\partial \theta_{0x}}\frac{\partial \eta_i}{\partial n_{\perp 0x}}\Big/\frac{\partial \phi_0}{\partial \theta_{0x}}\frac{\partial \eta_f}{\partial n_{\perp 0x}}\right). \tag{C16}$$

We have calculated the derivatives on the right-hand side of equations (C15) and (C16).

Using equation (C1) and (C3) (evaluated at $\xi_i = 3\theta_0/2$ and $\eta_i = \phi_0$), we find

$$\frac{\partial \xi_i}{\partial \theta_{0y}} = \frac{3}{2}; \quad \frac{\partial \xi_i}{\partial u_{0y}} = \frac{-\theta_{0y}}{2}; \quad \frac{\partial \eta_i}{\partial \theta_{0x}} = \frac{1}{\theta_{0y}}; \quad \frac{\partial \phi_0}{\partial \theta_{0x}} = \frac{1}{\theta_{0y}}; \quad \frac{\partial \eta_i}{\partial n_{\perp 0x}} = \frac{-2}{3\theta_{0y}}. \tag{C17}$$

Using Appendix B and equation (B2), we obtain (if $p_0 = \frac{1}{2}$):

$$\frac{\partial \xi_f}{\partial \theta_{0y}} = \frac{\theta_{yf}}{\theta_{0y}}\left\{\left(\frac{3}{2} - u_{yf}\right) + u_{yf}\left[\frac{(u_{yf} - u_+)(u_{yf} - u_-) - (u_{yf} - 3/2)(u_{yf} - 1)}{(u_{yf} - u_+)(u_{yf} - u_-) - u_{yf}(u_{yf} - 5/2)}\right]\right\}, \tag{C18}$$

$$\frac{\partial \xi_f}{\partial u_{0y}} = -\frac{2\theta_{yf}}{3\theta_{0y}}\left\{\left(\frac{3}{2} - u_{yf}\right) + \frac{5}{2}u_{yf}\left[\frac{(u_{yf} - u_+)(u_{yf} - u_-) - (u_{yf} - 3/2)(u_{yf} - 1)}{(u_{yf} - u_+)(u_{yf} - u_-) - u_{yf}(u_{yf} - 5/2)}\right]\right\}, \tag{C19}$$

$$\frac{\partial \eta_f}{\partial \theta_{0x}} = \frac{1}{\theta_{0y}}, \tag{C20}$$

$$\frac{\partial \eta_f}{\partial n_{\perp 0x}} = \frac{-1}{\theta_{0x} u_+ u_-}\left[u_{xf} - \frac{(u_{xf} - u_+)(u_{xf} - u_-)}{(u_{xf} - 3/2)}\right]. \tag{C21}$$

In the above, $u_+ = 3.581$ and $u_- = 0.419$.

Combining equations (C15)–(C21) yields for the low-frequency limit ($u_{xf} \rightarrow u_-$):

$$\left|\frac{\partial \Theta}{\partial \theta_0}\frac{\partial \Phi}{\partial \phi_0} - \frac{\partial \Theta}{\partial \phi_0}\frac{\partial \Phi}{\partial \theta_0}\right| = \frac{u_+}{2u_-} = 4.27\,. \tag{C22}$$

In the high-frequency regime ($p_0 = 1$) $\partial\Theta/\partial\theta_0 \rightarrow -3/2$ and $\partial\Phi/\partial\phi_0 \rightarrow -1$ so that

$$\left|\frac{\partial \Theta}{\partial \theta_0}\frac{\partial \Phi}{\partial \phi_0} - \frac{\partial \Theta}{\partial \phi_0}\frac{\partial \Phi}{\partial \theta_0}\right| = 1.50\,. \tag{C23}$$

APPENDIX D

CALCULATION OF VARIATION IN Ψ DUE TO FINITE WIDTH OF BEAMING ANGLE $\Delta\theta_b$

We wish to estimate the change in polarization position angle due to the finite angle $\Delta\theta_b$ over which the radiation is emitted. For simplicity we restrict ourselves to $\delta = 0$. A ray which is emitted along the field and is observed at $\delta = 0$ satisfies equations (58) and (59). We wish to calculate the change in position $\Delta\theta_{0x}$, and $\Delta\theta_{0y}$ and the change in initial direction $\Delta\xi_i$, and $\Delta\eta_i$ such that a ray emitted at an angle from the field of $\Delta\theta_b$ will be observed at a pulse longitude of $\delta = 0$, i.e. such that the change in final direction with respect to the magnetic axis ($\Delta\xi_f$, $\Delta\eta_f$) is zero.

Let

$$\Delta\theta_b^2 \equiv \Delta\theta_{bx}^2 + \Delta\theta_{by}^2\,. \tag{D1}$$

From the geometry $\Delta\theta_{bx} = \sin\,\xi_i(\Delta\eta_i - \Delta\phi_0)$ and $\Delta\theta_{by} = \Delta\xi_i - 3\Delta\theta_{0y}/2$. Assume $\Delta\theta_{bx}$ and $\Delta\theta_{by}$ are specified. Then (when $\theta_{0x} = 0$),

$$\Delta\xi_i = \Delta\theta_{by} + \frac{3}{2}\Delta\theta_{0y} \qquad \text{and} \qquad \Delta\eta_i = \frac{\Delta\theta_{bx}}{\sin\,\xi_i} + \frac{\Delta\theta_{0x}}{\theta_{0y}}\,. \tag{D2}$$

It is convenient to introduce the following notation:

$$\boldsymbol{U}_0 \equiv \begin{pmatrix} u_{0x} \\ u_{0y} \end{pmatrix} \quad \boldsymbol{\theta}_0 \equiv \begin{pmatrix} \theta_{0x} \\ \theta_{0y} \end{pmatrix} \quad \boldsymbol{D}_i \equiv \begin{pmatrix} \eta_i \\ \xi_i \end{pmatrix} \quad \boldsymbol{D}_f \equiv \begin{pmatrix} \eta_f \\ \xi_f \end{pmatrix} \quad \boldsymbol{\theta}_f \equiv \begin{pmatrix} \theta_{xf} \\ \theta_{yf} \end{pmatrix} \quad \delta\boldsymbol{\theta}_b \equiv \begin{pmatrix} \Delta\theta_{bx}/\sin\,\xi_i \\ \Delta\theta_{by} \end{pmatrix} \quad \boldsymbol{G} \equiv \begin{pmatrix} 1/\theta_{0y} & 0 \\ 0 & \frac{3}{2} \end{pmatrix}. \tag{D3}$$

From these definitions equation (D2) becomes $\delta\boldsymbol{D}_i = \delta\boldsymbol{\theta}_b + \boldsymbol{G}\cdot\delta\boldsymbol{\theta}_0$. We also note that the functional dependence of $\boldsymbol{\theta}_0$ and $\boldsymbol{D}_f$ as discussed in Appendix C is $\boldsymbol{\theta}_0 = \boldsymbol{\theta}_0(\boldsymbol{U}_0, \boldsymbol{D}_i)$ and $\boldsymbol{D}_f = \boldsymbol{D}_f(\boldsymbol{U}_0, \boldsymbol{\theta}_0)$. Thus,

$$\delta\boldsymbol{D}_f = \frac{\partial \boldsymbol{D}_f}{\partial \boldsymbol{U}_0}\cdot\delta\boldsymbol{U}_0 + \frac{\partial \boldsymbol{D}_f}{\partial \boldsymbol{\theta}_0}\cdot\delta\boldsymbol{\theta}_0\,, \tag{D4}$$

$$\delta\boldsymbol{\theta}_0 = \frac{\partial \boldsymbol{\theta}_0}{\partial \boldsymbol{U}_0}\cdot\delta\boldsymbol{U}_0 + \frac{\partial \boldsymbol{\theta}_0}{\partial \boldsymbol{D}_i}\cdot\delta\boldsymbol{D}_i\,, \tag{D5}$$

$$\delta\boldsymbol{D}_f = \left(\frac{\partial \boldsymbol{D}_f}{\partial \boldsymbol{U}_0} + \frac{\partial \boldsymbol{D}_f}{\partial \boldsymbol{\theta}_0}\frac{\partial \boldsymbol{\theta}_0}{\partial \boldsymbol{U}_0}\right)\cdot\delta\boldsymbol{U}_0 + \left[\frac{\partial \boldsymbol{D}_f}{\partial \boldsymbol{\theta}_0}\frac{\partial \boldsymbol{\theta}_0}{\partial \boldsymbol{D}_i}\right]\cdot\delta\boldsymbol{D}_i\,. \tag{D6}$$

Since we are interested in displacements in $\delta\boldsymbol{D}_i$, $\delta\boldsymbol{\theta}_0$ (and $\delta\boldsymbol{U}_0$) which yield zero for $\delta\boldsymbol{D}_f$, $\delta\boldsymbol{U}_0$ may be solved for

$$\delta\boldsymbol{U}_0 = -\left[\frac{\partial \boldsymbol{D}_f}{\partial \boldsymbol{U}_0} + \frac{\partial \boldsymbol{D}_f}{\partial \boldsymbol{\theta}_0}\frac{\partial \boldsymbol{\theta}_0}{\partial \boldsymbol{U}_0}\right]^{-1}\left[\frac{\partial \boldsymbol{D}_f}{\partial \boldsymbol{\theta}_0}\frac{\partial \boldsymbol{\theta}_0}{\partial \boldsymbol{D}_i}\right]\cdot\delta\boldsymbol{D}_i\,. \tag{D7}$$

so that $\delta\boldsymbol{\theta}_0$ becomes

$$\delta\boldsymbol{\theta}_0 = \left[\frac{\partial \boldsymbol{\theta}_0}{\partial \boldsymbol{U}_0}\cdot\left(\frac{\partial \boldsymbol{D}_f}{\partial \boldsymbol{U}_0} + \frac{\partial \boldsymbol{D}_f}{\partial \boldsymbol{\theta}_0}\frac{\partial \boldsymbol{\theta}_0}{\partial \boldsymbol{U}_0}\right)^{-1}\left(\frac{\partial \boldsymbol{D}_f}{\partial \boldsymbol{\theta}_0}\frac{\partial \boldsymbol{\theta}_0}{\partial \boldsymbol{D}_i}\right) + \frac{\partial \boldsymbol{\theta}_0}{\partial \boldsymbol{D}_i}\right]\cdot\delta\boldsymbol{D}_i\,. \tag{D8}$$

Substitution of equations (D2) and (D3) into (D8) and (D9) yields

$$\delta\boldsymbol{\theta}_0 = (\boldsymbol{I} - \boldsymbol{G})^{-1}\left[-\frac{\partial \boldsymbol{\theta}_0}{\partial \boldsymbol{U}_0}\cdot\left(\frac{\partial \boldsymbol{D}_f}{\partial \boldsymbol{U}_0} + \frac{\partial \boldsymbol{D}_f}{\partial \boldsymbol{\theta}_0}\frac{\partial \boldsymbol{\theta}_0}{\partial \boldsymbol{U}_0}\right)^{-1}\left(\frac{\partial \boldsymbol{D}_f}{\partial \boldsymbol{\theta}_0}\frac{\partial \boldsymbol{\theta}_0}{\partial \boldsymbol{D}_i}\right) + \frac{\partial \boldsymbol{\theta}_0}{\partial \boldsymbol{D}_i}\right]\cdot\delta\boldsymbol{\theta}_b\,, \tag{D9}$$

$$\delta\boldsymbol{U}_0 = -(\boldsymbol{I} - \boldsymbol{G})^{-1}\left(\frac{\partial \boldsymbol{D}_f}{\partial \boldsymbol{U}_0} + \frac{\partial \boldsymbol{D}_f}{\partial \boldsymbol{\theta}_0}\frac{\partial \boldsymbol{\theta}_0}{\partial \boldsymbol{U}_0}\right)^{-1}\left(\frac{\partial \boldsymbol{D}_f}{\partial \boldsymbol{\theta}_0}\frac{\partial \boldsymbol{\theta}_0}{\partial \boldsymbol{D}_i}\right)\cdot\delta\boldsymbol{\theta}_b\,. \tag{D10}$$

Finally we have

$$\Delta\theta_f = \frac{\partial\theta_f}{\partial \boldsymbol{U}_0}\cdot\delta\boldsymbol{U}_0 + \frac{\partial\theta_f}{\partial\boldsymbol{\theta}_0}\cdot\delta\boldsymbol{\theta}\,. \tag{D11}$$

Substitution of equations (D9) and (D10) into equation (D11), yields $\Delta\theta_{xf}$ and $\Delta\theta_{yf}$ in terms of $\Delta\theta_{bx}$ and $\Delta\theta_{by}$ which is the desired result. Calculation of $\partial \boldsymbol{D}_f/\partial\boldsymbol{U}_0$ and $\partial\boldsymbol{D}_f/\partial\boldsymbol{\theta}_0$ was done in Appendix C (eqs. [C12]–[C14] and [C18]–[C21]).

Other derivatives that are needed are

$$\frac{\partial\theta_{xf}}{\partial\theta_{0x}} = \frac{\theta_{yf}}{\theta_{0y}}\,,\quad \frac{\partial\theta_{xf}}{\partial\theta_{0y}} = 0\,,\quad \frac{\partial\theta_{yf}}{\partial\theta_{0x}} = 0\,,\quad \frac{\partial\theta_{yf}}{\partial\theta_{0y}} = \frac{\theta_{yf}}{\theta_{0y}}\left[1 + \frac{3(u_{yf}-1)\partial u_{yf}/\partial u_{0y}}{5(u_{yf}-u_+)(u_{yf}-u_-)}\right]; \tag{D12}$$

$$\frac{\partial\theta_{xf}}{\partial u_{0x}} = 0\,,\quad \frac{\partial\theta_{xf}}{\partial u_{0y}} = 0\,,\quad \frac{\partial\theta_{yf}}{\partial u_{0x}} = 0\,,\quad \frac{\partial\theta_{yf}}{\partial u_{0y}} = \theta_{yf}\left[\frac{-(u_{yf}-1)\partial u_{yf}/\partial u_{0y}}{(u_{yf}-u_+)(u_{yf}-u_-)} - \frac{2}{3}\right]. \tag{D13}$$

Above

$$\frac{\partial u_{yf}}{\partial u_{0y}} = \frac{5u_{yf}(u_{yf}-u_+)(u_{yf}-u_-)}{3[(u_{yf}-u_+)(u_{yf}-u_-) - u_{yf}(u_{yf}-5/2)]}\,.$$

From the definitions of ξ_i and η_i in Appendix C we have

$$\begin{aligned}
&\frac{\partial\theta_{0x}}{\partial\xi_i} = 0\,,\quad \frac{\partial\theta_{0x}}{\partial\eta_i} = \theta_{0y}\,,\quad \frac{\partial\theta_{0x}}{\partial u_{0x}} = 0\,,\quad \frac{\partial\theta_{0x}}{\partial u_{0y}} = 0\,;\\
&\frac{\partial\theta_{0y}}{\partial\xi_i} = \frac{2}{3}\,,\quad \frac{\partial\theta_{0y}}{\partial\eta_i} = 0\,,\quad \frac{\partial\theta_{0y}}{\partial u_{0x}} = 0\,,\quad \frac{\partial\theta_{0y}}{\partial u_{0y}} = \frac{2}{3}\,\theta_{0y}\,.
\end{aligned} \tag{D14}$$

Note that all of equations (D12)–(D14) were evaluated with $u_{0x} = u_{0y} = \theta_{0x} = \eta_i = \eta_f = 0$. Evaluation of equation (D11) using equations (D9)–(D10), and (D12) yields an x-component of $\Delta\theta_f$ of

$$\Delta\theta_{xf} = \frac{\theta_{yf}}{\theta_{0y}}\left(\frac{u_{xf}-1}{u_+\,u_-}\right)\Delta\theta_{bx}\,. \tag{D15}$$

Use of equations (60) and (63) in the text then yield the desired $\Delta\psi$, equation (64).

REFERENCES

Arons, J. 1981, *Ap. J.*, **248**, 1099.
———. 1983*a*, *Ap. J.*, **266**, 215.
———. 1983*b*, in *Positron-Electron Pairs in Astrophysics*, ed. M. L. Burns, A. K. Harding, and R. Ramaty (New York: AIP), p. 163.
Arons, J., and Barnard, J. J. 1986, *Ap. J.*, **303**, 137 (Paper I).
Arons, J., and Scharlemann, E. T. 1979, *Ap. J.*, **231**, 854 (AS).
Backer, D. C. 1976, *Ap. J.*, **209**, 895.
Backer, D. C., and Rankin, J. M. 1980, *Ap. J. Suppl.*, **42**, 143.
Backer, D. C., Rankin, J. M., and Campbell, D. B. 1976, *Nature*, **263**, 202.
Barnard, J. J. 1986, *Ap. J.*, **303**, in press.
Barnard, J. J., and Arons, J. 1982, *Ap. J.*, **254**, 713.
Bartel, N. 1981, *Astr. Ap.*, **97**, 384.
Bekefi, G. 1966, *Radiation Processes in Plasmas* (New York: Wiley).
Blandford, R. D., and Scharlemann, E. T. 1976, *M.N.R.A.S.*, **174**, 59.
Budden, K. G. 1961, *Radio Waves in the Ionosphere* (Cambridge: Cambridge University Press).
Cheng, A. F., and Ruderman, M. A. 1977, *Ap. J.*, **214**, 598.
———. 1979, *Ap. J.*, **229**, 348.
———. 1980, *Ap. J.*, **235**, 576.
Cordes, J. M. 1978, *Ap. J.*, **235**, 576.
———. 1979, *Australian J. Phys.*, **32**, 9.
Cordes, J. M., and Stinebring, D. 1984, *Ap. J. (Letters)*, **277**, L53.
Fawley, W. 1978, Ph.D. thesis, University of California, Berkeley.
Goldreich, P., and Julian, W. H. 1969, *Ap. J.*, **157**, 869.
Harding, A. K., and Tademaru, E. 1981, *Ap. J.*, **243**, 597.
Komesaroff, M. M. 1970, *Nature*, 612.
Lee, M. A., and Lerche, I. 1975, *Ap. J.*, **198**, 477.
Malofeev, V. M., and Malov, I. F. 1980, *Astr. Zh.*, **57**, 90 (English transl. *Soviet Astr.*, **24**, 54 [1980]) (MM).
Manchester, R. N., and Taylor, J. H. 1977, *Pulsars* (San Francisco: Freeman).
Manchester, R. N., Taylor, J. H., and Huguenin, C. R. 1975, *Ap. J.*, **196**, 83.
Melrose, D. B. 1979, *Australian J. Phys.*, **32**, 61.
Melrose, D. B., and Stoneham, R. J. 1977, *Proc. Astr. Soc. Australia*, **3**, 120.
Ostriker, J. P., and Gunn, J. E. 1969, *Ap. J.*, **157**, 1395.
Radhakrishnan, V., and Cooke, D. J. 1969, *Ap. Letters*, **3**, 225 (RC).
Rankin, J. M. 1983*a*, *Ap. J.*, **274**, 333.
———. 1983*b*, *Ap. J.*, **274**, 359.
Rickett, B. J., and Cordes, J. M. 1981, in *IAU Symposium 95, Pulsars*, ed. W. Sieber and R. Wielebinskii (Dordrecht: Reidel), p. 107.
Ruderman, M. A., and Sutherland, P. G. 1975, *Ap. J.*, **196**, 51 (RS).
Sieber, W., Reinecke, R., and Wielebinski, R. 1975, *Astr. Ap.*, **38**, 169.
Stinebring, D. 1982, Ph.D. thesis, Cornell University.
Stinebring, D., Cordes, J. M., Rankin, J. M., Weisberg, J. M., and Boriakoff, V. 1984*a*, *Ap. J. Suppl.*, **55**, 247.
———. 1984*b*, *Ap. J. Suppl.*, **55**, 279.
Sturrock, P. 1970, *Nature*, **227**, 465.
———. 1971, *Ap. J.*, **164**, 529.
Weinberg, S. 1962, *Phys. Rev.*, **126**, 1899.

J. Arons: Department of Astronomy, 601 Campbell Hall, University of California, Berkeley, CA 94720

J. J. Barnard: Laboratory for High Energy Astrophysics, Code 665, NASA-Goddard Space Flight Center, Greenbelt, MD 20771